LETTER

doi:10.1038/nature19346

The long non-coding RNA *Morrbid* regulates *Bim* and short-lived myeloid cell lifespan

Jonathan J. Kotzin[1,2*], Sean P. Spencer[1,2*†], Sam J. McCright[1,2], Dinesh B. Uthaya Kumar[3,4], Magalie A. Collet[3], Walter K. Mowel[1,2], Ellen N. Elliott[3], Asli Uyar[3], Michelle A. Makiya[5], Margaret C. Dunagin[6], Christian C. D. Harman[7,8], Anthony T. Virtue[1,2], Stella Zhu[3], Will Bailis[7], Judith Stein[7,8], Cynthia Hughes[7,8], Arjun Raj[6], E. John Wherry[2,9], Loyal A. Goff[10,11], Amy D. Klion[5], John L. Rinn[12,13], Adam Williams[3,4], Richard A. Flavell[7,8] & Jorge Henao-Mejia[1,2,14]

Neutrophils, eosinophils and 'classical' monocytes collectively account for about 70% of human blood leukocytes and are among the shortest-lived cells in the body[1,2]. Precise regulation of the lifespan of these myeloid cells is critical to maintain protective immune responses and minimize the deleterious consequences of prolonged inflammation[1,2]. However, how the lifespan of these cells is strictly controlled remains largely unknown. Here we identify a long non-coding RNA that we termed *Morrbid*, which tightly controls the survival of neutrophils, eosinophils and classical monocytes in response to pro-survival cytokines in mice. To control the lifespan of these cells, *Morrbid* regulates the transcription of the neighbouring pro-apoptotic gene, *Bcl2l11* (also known as *Bim*), by promoting the enrichment of the PRC2 complex at the *Bcl2l11* promoter to maintain this gene in a poised state. Notably, *Morrbid* regulates this process in *cis*, enabling allele-specific control of *Bcl2l11* transcription. Thus, in these highly inflammatory cells, changes in *Morrbid* levels provide a locus-specific regulatory mechanism that allows rapid control of apoptosis in response to extracellular pro-survival signals. As *MORRBID* is present in humans and dysregulated in individuals with hypereosinophilic syndrome, this long non-coding RNA may represent a potential therapeutic target for inflammatory disorders characterized by aberrant short-lived myeloid cell lifespan.

Neutrophils, eosinophils and 'classical' monocytes represent a first line of defense against nearly all pathogens[1,2]. However, these short-lived myeloid cells also contribute to the development of several inflammatory diseases[1,2]. Cytokines and metabolites tightly regulate the function and lifespan of these cells, but how these cues are translated into an optimal cellular lifespan is largely unknown. Emerging evidence indicates that certain long non-coding RNAs (lncRNAs) can integrate extracellular inputs with chromatin-modification pathways allowing cells to rapidly adapt to their environment[3,4]. As such, we investigated whether lncRNAs control the function or lifespan of short-lived myeloid cells in response to extracellular cues. We first analysed multiple RNA sequencing (RNA-seq) datasets for mouse lncRNAs that are preferentially expressed by mature short-lived myeloid cells[5,6]. We identified an uncharacterized lncRNA (*Gm14005*) that we termed *Morrbid* (myeloid RNA regulator of Bim-induced death). *Morrbid* is conserved across species, contains five exons, is poly-adenylated and is localized predominately to the nucleus bound to chromatin (Fig. 1a, b, Extended Data Fig. 1a–d). Importantly, *Morrbid* is highly and specifically expressed by mature eosinophils, neutrophils and classical monocytes in both mice and humans (Fig. 1c, d, Extended Data Fig. 1e, f).

To investigate the role of *Morrbid in vivo*, we deleted the *Morrbid* locus to generate *Morrbid*-deficient mice (Extended Data Fig. 1g). Notably, and in accordance with the expression profile of *Morrbid*, we found that eosinophils, neutrophils and Ly6C^{hi} classical monocytes were markedly reduced in the blood and tissues of these mice (Fig. 1e, Extended Data Fig. 1h, i). This defect was highly specific to these three cell types, as well as blood Ly6C^{lo} monocytes (Extended Data Fig. 2a), which are suggested to be progeny of Ly6C^{hi} monocytes[7]. All other lymphoid and myeloid cell types were unaffected (Extended Data Fig. 1i, 2a). Similarly, knockdown of *Morrbid in vivo* also led to a specific reduction in the frequency of short-lived myeloid cells in blood and spleen (Extended Data Fig. 2b–e). Finally, as these cells have a critical role in protective immunity and in the development of immunopathology, we found that *Morrbid*-deficient mice were highly susceptible to bacterial (*Listeria monocytogenes*) infection (Fig. 1f, g), and protected from eosinophil-driven allergic lung inflammation (Extended Data Fig. 2f–h). Altogether, these results support an important and selective role for *Morrbid* and potentially DNA elements within its locus in short-lived myeloid cell homeostasis.

Eosinophils, neutrophils and Ly6C^{hi} monocytes originate from common progenitors in the bone marrow (BM)[1,8], with extracellular cues driving the developmental programs needed to produce each of these cell types[1,8]. Using mixed BM chimaeras, we found that *Morrbid*-deficient BM cells have a significant defect in the generation of short-lived myeloid cells (Extended Data Fig. 3a–e), indicating that *Morrbid* acts in a cell-intrinsic manner. We next sought to determine whether *Morrbid* regulates short-lived myeloid cell development. Early progenitors of each of these cell types express low levels of *Morrbid* and its expression increases throughout development to reach maximal levels in fully mature eosinophils, neutrophils and Ly6C^{hi} monocytes (Extended Data Fig. 3f–h). In accordance with this pattern of expression, the progenitors of each of these cell types were intact in *Morrbid*-deficient mice (Fig. 2a, Extended Data Fig. 3g–h). These results suggest that *Morrbid* regulates the frequency of mature eosinophils, neutrophils and monocytes, but not their progenitors.

Mature populations of myeloid cells are controlled by several mechanisms, including homeostatic proliferation, trafficking, and cell death. We found no defects in homeostatic proliferation in *Morrbid*-deficient mice (Extended Data Fig. 4a). Mature short-lived myeloid cells are

[1]Department of Pathology and Laboratory Medicine, University of Pennsylvania, Philadelphia, Pennsylvania 19104, USA. [2]Institute for Immunology, Perelman School of Medicine, University of Pennsylvania, Philadelphia, Pennsylvania 19104, USA. [3]The Jackson Laboratory for Genomic Medicine, Farmington, Connecticut 06032, USA. [4]Department of Genetics and Genomic Sciences, University of Connecticut Health Center, Farmington, Connecticut 06032, USA. [5]Laboratory of Parasitic Diseases, National Institute of Allergy and Infectious Diseases, National Institutes of Health, Bethesda, Maryland 20892, USA. [6]Department of Bioengineering, University of Pennsylvania, Philadelphia, Pennsylvania 19104, USA. [7]Department of Immunobiology, Yale University School of Medicine, New Haven, Connecticut 06520, USA. [8]Howard Hughes Medical Institute, Yale University, New Haven, Connecticut 06510, USA. [9]Department of Microbiology, Perelman School of Medicine, University of Pennsylvania, Philadelphia, Pennsylvania 19104, USA. [10]McKusick-Nathans Institute of Genetic Medicine, Johns Hopkins University, Baltimore, Maryland 21205, USA. [11]Department of Neuroscience, Johns Hopkins University, Baltimore, Maryland 21205, USA. [12]Biological and Biomedical Sciences, Harvard Medical School, Boston, Massachusetts 02115, USA. [13]Department of Stem Cell and Regenerative Biology, Harvard University, Cambridge, Massachusetts 02138, USA. [14]Division of Transplant Immunology, The Children's Hospital of Philadelphia, Philadelphia, Pennsylvania 19104, USA. †Present address: Department of Medicine, Massachusetts General Hospital, 55 Fruit St, Boston, Massachusetts 02114, USA.
*These authors contributed equally to this work.

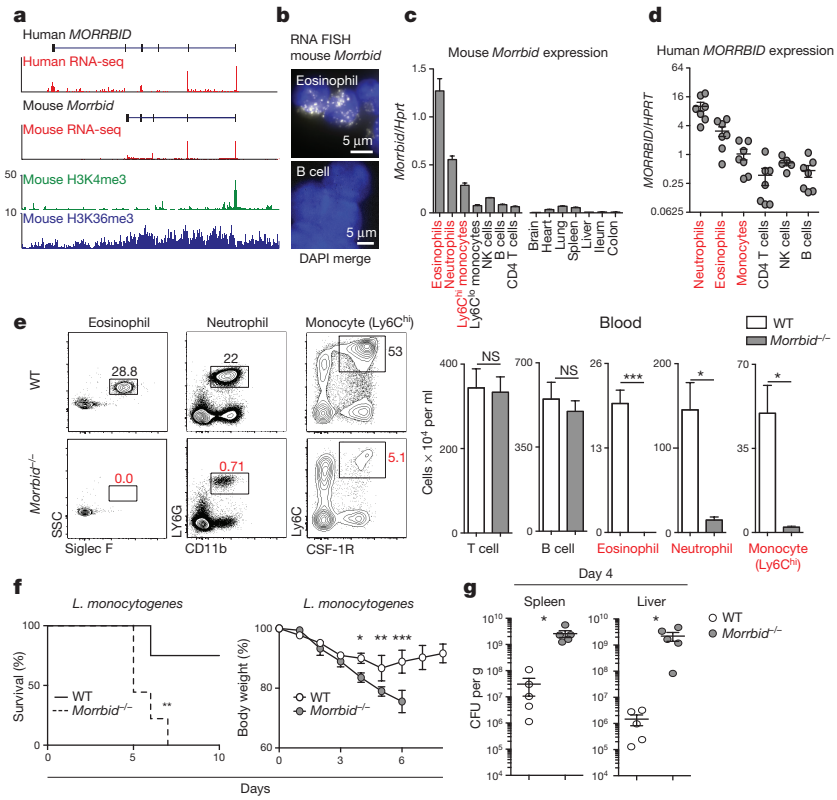

Figure 1 | lncRNA *Morrbid* is a critical regulator of eosinophils, neutrophils and Ly6C^{hi} monocytes. a, Human neutrophil and mouse granulocyte normalized RNA-seq and ChIP–seq tracks at the *Morrbid* locus. **b**, Single molecule *Morrbid* RNA fluorescence *in situ* hybridization (FISH). **c**, **d**, qPCR expression of mouse ($n = 3$; representative of 3 independent experiments) (**c**) and human *Morrbid* in indicated cell types and tissues ($n = 7$) (**d**). **e**, Wild-type and *Morrbid*-deficient flow cytometry plots and absolute counts ($n = 3$–5; representative of 7 independent experiments). **f**, **g**, *L. monocytogenes* infection of wild-type and *Morrbid*-deficient mice. **f**, Survival and weight loss ($n = 9$, representative of 3 independent experiments). **g**, Colony-forming units (CFUs) per g from indicated organs ($n = 5$; representative of 3 independent experiments). Error bars show s.e.m. $^{*}P < 0.05$, $^{**}P < 0.01$, and $^{***}P < 0.001$ (two-sided *t*-test, **e**, **g**, **f** (right); Mantel–Cox test, **f** (left)).

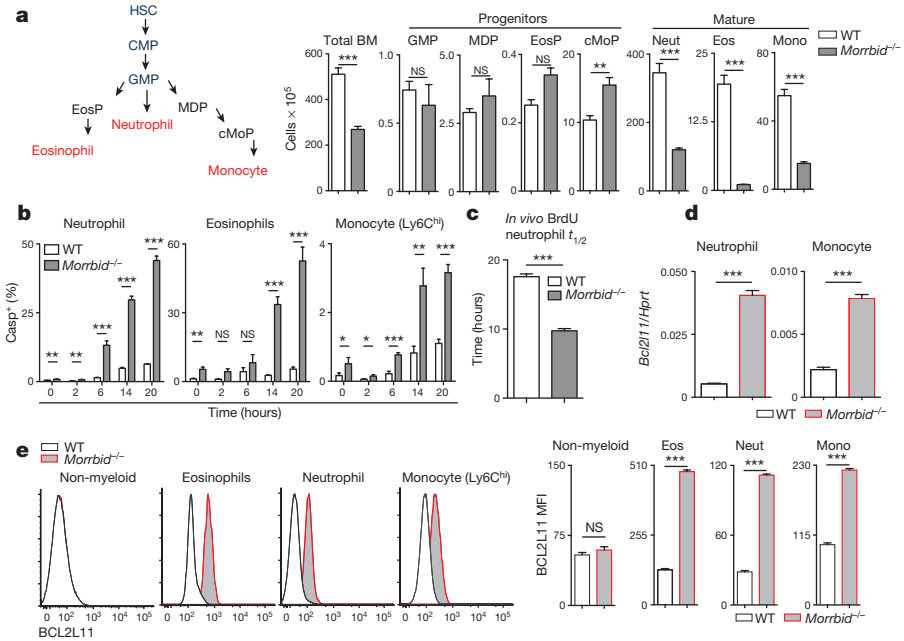

Figure 2 | *Morrbid* controls eosinophil, neutrophil and Ly6C^{hi} monocyte lifespan. a, Schematic of short-lived myeloid cell development and absolute numbers of the indicated cell types in BM from wild-type and *Morrbid*-deficient mice ($n = 3$–5; representative of 3 independent experiments). **b**, Frequency of Casp^{+} (Z-VAD-FMK^{+}) cultured BM cells ($n = 3$ mice; representative of 2 independent experiments). **c**, Half-life of BrdU pulse-labelled neutrophils in blood *in vivo* ($n = 4$ mice; representative of 3 independent experiments). **d**, *Bcl2l11* qPCR expression in indicated cell types sorted from BM ($n = 3$; representative of 2 independent experiments). **e**, BCL2L11 protein expression assessed by flow cytometry in indicated BM cell types. Left, representative histograms. Right, mean fluorescence intensity (MFI) quantification ($n = 3$–5 mice, representative of 3 independent experiments). Error bars show s.e.m. $^{*}P < 0.05$, $^{**}P < 0.01$ and $^{***}P < 0.001$ (two-sided *t*-test).

substantially reduced in the BM of *Morrbid*-deficient mice and there was a near absence of *in vitro* BM-differentiated eosinophils[9] (Fig. 2a, Extended Data Fig. 4b, c), suggesting that *Morrbid* controls a dominant process independent of cell trafficking. Notably, *Morrbid*-deficient eosinophils, neutrophils and Ly6C^{hi} monocytes were all highly prone to apoptosis in BM cultured *ex vivo* (Fig. 2b, Extended Data Fig. 4d). Furthermore, we observed significantly increased apoptosis *in vitro* in BM-derived eosinophils (Extended Data Fig. 4e), and *in vivo* during *L. monocytogenes* infection in the absence of *Morrbid* (Extended Data Fig. 4f). Given the close relationship between apoptosis and cellular lifespan, we hypothesized that *Morrbid* is a regulator of short-lived myeloid cell half-life. Using BrdU to label circulating neutrophils and determine their decay rate, we observed an ~2-fold decrease in the half-life of these cells (Fig. 2c, Extended Data Fig. 4g). These results indicate that *Morrbid* regulates short-lived myeloid cell lifespan through control of apoptosis.

Some lncRNAs regulate the expression of neighbouring genes[10–13]. The pro-apoptotic gene *Bcl2l11* (*Bim*) is located ~150-kb downstream of *Morrbid* (Extended Data Fig. 1a). *Bcl2l11* has been shown to be an important regulator of myeloid homeostasis[14,15]. Thus, we reasoned that *Morrbid* regulates short-lived myeloid cell lifespan through its control of *Bcl2l11* expression. Indeed, the protein and mRNA levels of *Bcl2l11* were markedly elevated in eosinophils, neutrophils and Ly6C^{hi} monocytes from *Morrbid*-deficient mice (Fig. 2d, e, Extended Data Fig. 4h–k). In concordance with the pattern of *Morrbid* expression, *Bcl2l11* was maximally elevated in the mature state of each of these cell lineages in *Morrbid*-deficient mice (Extended Data Fig. 4l), and was not dysregulated in other myeloid and lymphoid cell populations (Extended Data Fig. 4m). Importantly, key myeloid lineage transcription factors and other genes neighbouring *Morrbid* were largely unaffected in the absence of *Morrbid* (Extended Data Fig. 5a–c). These results suggest that *Morrbid* represses *Bcl2l11* expression in short-lived myeloid cells.

To specifically address the role of *Morrbid* RNA in the regulation of *Bcl2l11* expression, we first established an *in vitro* eosinophil culture system in which we could study the function of *Morrbid* RNA in the absence of genetic disruptions[9] (Extended Data Fig. 6a). Using this system, we found that short hairpin RNA (shRNA)-mediated knockdown of *Morrbid* RNA results in a significant elevation in BCL2L11, which was accompanied by a substantial decrease in eosinophil survival (Figure 3a–c, Extended Data Fig. 6b–d). We observed similar results using transfection of locked nucleic acids (LNAs) as an independent knockdown technique (Extended Data Fig. 6e). We next sought to corroborate these results in a different cell type within the myeloid cell lineage. Interestingly, we found that lipopolysaccharide (LPS)-stimulated BM-derived macrophages (BMDMs) highly upregulated *Morrbid* (Extended Data Fig. 6f). Notably, LNA knockdown of *Morrbid,* deletion of the *Morrbid* promoter, or deletion of its locus in LPS-stimulated BMDMs resulted in a marked increase in *Bcl2l11* expression and apoptosis (Extended Data Fig. 6f–l). Altogether, these results indicate that *Morrbid* RNA is a critical regulator of *Bcl2l11* expression and short-lived myeloid cell survival.

Pro-survival cytokines can potently influence the lifespan of immune cells. One well-described mechanism of this control is through the repression of *Bcl2l11* (refs 15, 16). We hypothesized that cytokines from the common β-chain receptor family (IL-3, IL-5 and GM-CSF), which are known to promote the survival of eosinophils, neutrophils and Ly6C^{hi} monocytes, regulate *Bcl2l11* expression through the induction of *Morrbid*. To test this hypothesis, we first withdrew cytokines from cultured BM-derived eosinophils and observed a loss of *Morrbid* expression and an increase in *Bc2l11* levels (Fig. 3d). Subsequent addition of IL-5, IL-3 or GM-CSF induced *Morrbid* expression, which was accompanied by *Bcl2l11* repression (Fig. 3d). Similarly, *ex-vivo* β-chain cytokine stimulation, but not G-CSF stimulation, significantly induced *Morrbid* and a corresponding repression of *Bcl2l11* in neutrophils and Ly6C^{hi} monocytes (Fig. 3e, Extended Data Fig. 6m). Importantly, *Morrbid*-deficient neutrophils were unable to inhibit *Bcl2l11* expression

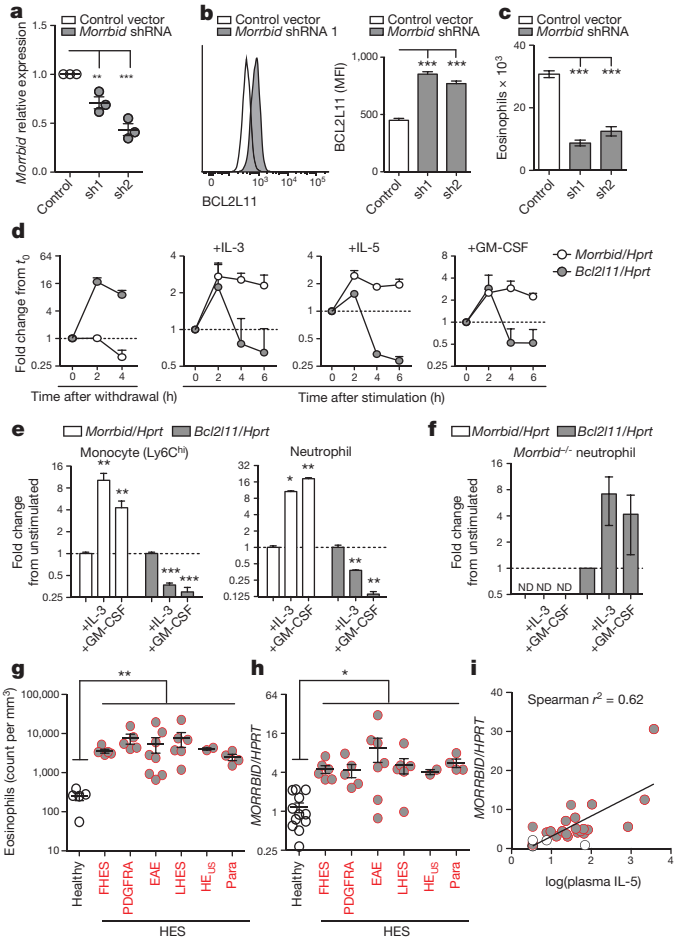

Figure 3 | Pro-survival cytokines repress pro-apoptotic *Bcl2l11* through induction of *Morrbid* RNA. a–c, BM-derived eosinophils transduced with control or *Morrbid*-specific shRNAs. **a**, *Morrbid* qPCR expression. **b**, **c**, BCL2L11 protein expression (**b**) and absolute eosinophil counts (**c**) ($n = 3$ mice per group, representative of 2 independent experiments). **d**, *Morrbid* and *Bcl2l11* qPCR expression in BM-derived eosinophils following withdrawal/stimulation with indicated cytokines ($n = 3$ mice, representative of 2 independent experiments). **e**, **f**, *Morrbid* and *Bcl2l11* qPCR expression in wild-type (**e**) and *Morrbid*-deficient (**f**) sorted BM cell types stimulated with indicated cytokines ($n = 3$–4 mice, representative of 3 independent experiments). **g–i**, *MORRBID* expression in human hypereosinophilic syndrome (HES). Absolute eosinophil count (**g**), purified eosinophil *MORRBID* qPCR expression (**h**), and correlation between log(plasma IL-5) and *MORRBID* expression (**i**) (each dot represents one individual; $n = 2$–12 per disease group). FHES, familial HES; PDGFRA, PDGFRA^{+} HES; EAE, episodic angioedema and eosinophilia; LHES, lymphocytic variant HES; HEus, HES of undetermined significance; Para, parasitic infection. Error bars show s.e.m. $^{*}P < 0.05$, $^{**}P < 0.01$, and $^{***}P < 0.001$ (two-sided *t*-test, **a–h**; Spearman's correlation, **i**).

upon addition of β-chain cytokines (Fig. 3f). These results suggest that β-chain cytokines repress *Bcl2l11* expression in short-lived myeloid cells in a *Morrbid*-dependent manner.

Dysregulated immune cell survival is central to many human haematological and inflammatory diseases. Hypereosinophilic syndrome (HES) is a group of disorders characterized by eosinophilia and a wide range of clinical manifestations[17]. Several HES subtypes have been associated with increased production or responsiveness to IL-5 (ref. 17). We therefore reasoned that eosinophils from individuals with HES would overexpress *MORRBID*, and that this overexpression would positively correlate with IL-5 levels. We screened patients with varied subtypes of HES (Fig. 3g), and found that eosinophils from these patients expressed significantly higher levels of *MORRBID* than that of

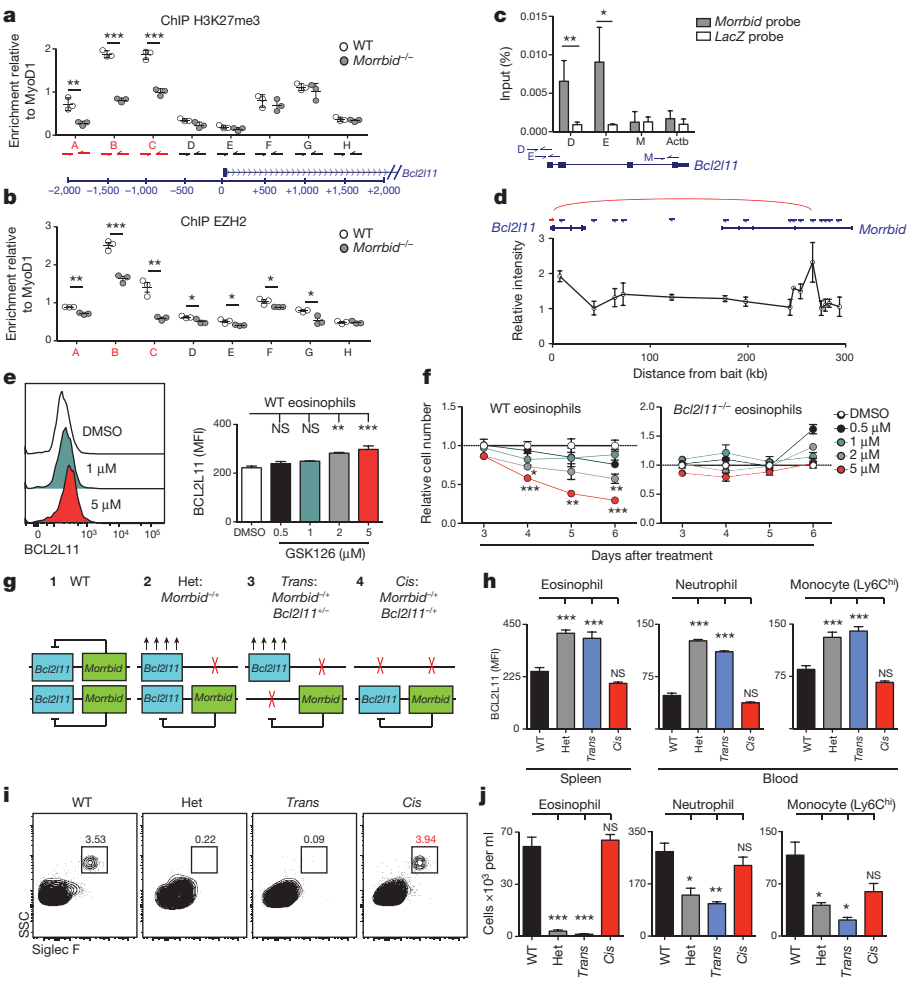

Figure 4 | *Morrbid* represses *Bcl2l11* in *cis* by maintaining its bivalent promoter in a poised state. **a**, **b**, ChIP–qPCR for H3K27me3 (**a**) and EZH2 (**b**) at the *Bcl2l11* promoter in sorted BM neutrophils (dots represents 1–2 pooled mice). **c**, ChIRP–qPCR of *Morrbid* RNA occupancy. D, E and M represent selected qPCR primer locations within the *Bcl2l11* locus as indicated by the gene schematic (average of 3 independent experiments). **d**, 3C of the *Bcl2l11* promoter and indicated genomic regions (average of 3 independent experiments). **e**, **f**, Wild-type and *Bcl2l11*-deficient BM-derived eosinophils treated with the EZH2 inhibitor GSK126. **e**, BCL2L11 protein expression on treatment day 5. **f**, Number of cells relative to DMSO treatment control ($n = 3$ mice per dose, representative of 2 independent experiments). **g**–**j**, Allele-specific combinations of *Morrbid*- and *Bcl2l11*-deficient mice. **g**, Schema of generated allele-specific mutant mice. **h**, Quantification of BCL2L11 MFI of indicated cell types. **i**, Representative flow cytometry of blood eosinophils. **j**, Absolute counts of indicated splenic cell types ($n = 3$–9 mice per group). Error bars show s.e.m. $^{*}P < 0.05$, $^{**}P < 0.01$, and $^{***}P < 0.001$ (two-sided *t*-test, **a**–**c**; one-way ANOVA with Tukey post-hoc test, **e**, **f**, **h**, **j**).

healthy controls (Fig. 3h). Additionally, we observed that *MORRBID* expression in eosinophils was positively correlated with plasma IL-5 levels (Fig. 3i). These results suggest a potential role for *MORRBID* in HES and other inflammatory diseases characterized by high levels of β-chain cytokines and altered short-lived myeloid cell lifespan.

Genes that require both tight regulation and the ability to be rapidly activated frequently have activating (H3K4me3) and repressive (H3K27me3) histone marks in their promoters, termed bivalent promoters[18]. The *Bcl2l11* gene has previously been described as having a bivalent promoter, which allows this pro-apoptotic gene to be maintained in a poised state[19]. A number of lncRNAs have been shown to repress gene expression by promoting the enrichment of polycomb repressive complex 2 (PRC2) at target genes, which in turn catalyzes the deposition of H3K27me3 (refs 20, 21). We therefore hypothesized that *Morrbid* represses *Bcl2l11* expression and prevents short-lived myeloid cell apoptosis by promoting PRC2 enrichment and H3K27me3 deposition at the bivalent promoter of *Bcl2l11*.

To test this hypothesis, we first performed chromatin immunoprecipitation followed by quantitative PCR (ChIP–qPCR) for total polymerase II (Pol II), H3K27me3 and the PRC2 subunit EZH2 in neutrophils from wild-type and *Morrbid*-deficient mice. In line with the elevated levels of *Bcl2l11* in *Morrbid*-deficient cells, we found that Pol II occupancy was significantly increased (Extended Data Fig. 7a), and the levels of H3K27me3 and EZH2 were markedly reduced at the promoter of *Bcl2l11* in the absence of *Morrbid* (Fig. 4a, b). We next asked whether the induction of *Morrbid* expression promotes the accumulation of PRC2 at the *Bcl2l11* promoter. Using the BMDM system in which *Morrbid* is induced upon LPS stimulation, we found that *Morrbid* levels and EZH2 occupancy at the *Bcl2l11* promoter concurrently increase in a *Morrbid*-dependent manner (Extended Data Fig. 7b). Finally, using ChIP–seq and ATAC–seq (assay for transposase-accessible chromatin using sequencing), we did not detect changes in the activating histone marks H3K4me1 and H3K4me3, and only a modest increase in chromatin accessibility at the *Bcl2l11* promoter in the absence of *Morrbid* (Extended Data Fig. 7c–f). Altogether, these results indicate that *Morrbid* represses *Bcl2l11* expression in short-lived myeloid cells by promoting the deposition of H3K27me3 at the bivalent promoter of *Bcl2l11*.

lncRNAs have been suggested to promote the recruitment of PRC2 to target genes through direct lncRNA–PRC2 interactions or indirect mechanisms[11,20–24]. To understand further the mechanism by which *Morrbid* promotes PRC2 enrichment at the *Bcl2l11* promoter, we first examined whether *Morrbid* RNA associates with PRC2. Using a recently generated EZH2 photoactivatable ribonucleoside-enhanced crosslinking and immunoprecipitation (PAR–CLIP) dataset[22], we found that *Morrbid* associates with EZH2 (Extended Data Fig. 8a). To further support this association, we performed RNA immunoprecipitation against EZH2 in myeloid cells and found that *Morrbid* significantly co-immunoprecipitates with this PRC2 subunit (Extended Data Fig. 8b). We next asked whether *Morrbid* RNA associates with chromatin regions within the *Bcl2l11* promoter, with which PRC2 also associates. We performed chromatin isolation by RNA purification (ChIRP)–qPCR in LPS-treated BMDMs. Using DNA probes that specifically and robustly retrieved *Morrbid* RNA (Extended Data Fig. 8c), we found that *Morrbid* association with chromatin was significantly enriched at the *Bcl2l11* promoter (Fig. 4c). Finally, we asked how *Morrbid* RNA comes into proximity of the *Bcl2l11* promoter. A number of lncRNA genes have been reported to loop into proximity with the genes that they regulate[10–13,25]; thus, we reasoned that the *Morrbid* and *Bcl2l11* loci interact with one another through DNA

looping. Using chromosome conformation capture (3C), we indeed observed a long-distance association between *Bcl2l11* and the *Morrbid* locus in short-lived myeloid cells (Fig. 4d, Extended Data Fig. 8d). Altogether, these results suggest a model in which *Morrbid* proximity to *Bcl2l11*, mediated through DNA looping, enables *Morrbid* RNA to promote PRC2 enrichment within the *Bcl2l11* promoter through direct *Morrbid*–PRC2 interactions and potentially through additional indirect mechanisms.

Our findings suggest an important role for PRC2 in *Morrbid*-dependent repression of *Bcl2l11*. Yet, whether short-lived myeloid cell survival depends on PRC2-mediated transcriptional repression of *Bcl2l11* is not known. We cultured eosinophils in the presence of a specific inhibitor of EZH2, GSK126. We observed a dose-dependent increase in BCL2L11 and eosinophil apoptosis upon PRC2 inhibition (Fig. 4e, f, Extended Data Fig. 8e, f). Importantly, *Bcl2l11*-deficient eosinophils were resistant to cell death following abrogation of PRC2 activity (Fig. 4f, Extended Data Fig. 8e, f). Altogether, these results demonstrate that PRC2 regulates short-lived myeloid cell survival specifically through repression of *Bcl2l11* expression, further supporting a critical role for *Morrbid* in the regulation of the lifespan of these highly inflammatory cells.

Finally, we found that *Morrbid*-heterozygous mice largely recapitulated the phenotype of mice lacking both alleles of *Morrbid* (Extended Data Fig. 8g). In light of this dominant heterozygous phenotype and the observed *Morrbid-Bcl2l11* DNA loop, we hypothesized that *Morrbid* functions in *cis* to repress *Bcl2l11*. As such, we expected that deletion of *Bcl2l11* on the same chromosome as that of the *Morrbid*-deficient allele will normalize *Bcl2l11* expression in short-lived myeloid cells and rescue their numbers, but that deletion of *Bcl2l11* on the opposite chromosome would not (Fig. 4g). We therefore generated all permutations of *Morrbid* and *Bcl2l11* double-heterozygous mice (Extended Data Fig. 9). Notably, deletion of *Bcl2l11* in *cis*, but not in *trans*, of the *Morrbid*-deficient allele normalized *Bcl2l11* expression (Fig. 4h) and rescued short-lived myeloid cell numbers (Fig. 4i, j, Extended Data Fig. 10a, b). Other cell types were largely unaltered in these genetic backgrounds (Extended Data Fig. 10b–d). This complete rescue in *cis* double-heterozygous mice indicates that *Morrbid* acts in an allele-specific manner to regulate *Bcl2l11* expression and short-lived myeloid cell lifespan.

Here we show that *Morrbid* integrates extracellular signals to control the lifespan of eosinophils, neutrophils and monocytes through allele-specific suppression of *Bcl2l11* expression (Extended Data Fig. 10e). As this lncRNA is present in humans and dysregulated in patients with HES, a better understanding of how *Morrbid* RNA and potentially DNA elements within its locus regulate *Bcl2l11* may provide new therapeutic approaches for several human inflammatory diseases. Finally, our results demonstrate that lncRNAs can function as highly cell-type specific local effectors of extracellular cues to control immunological processes that require rapid and strict regulation.

Online Content Methods, along with any additional Extended Data display items and Source Data, are available in the online version of the paper; references unique to these sections appear only in the online paper.

Received 18 December 2015; accepted 8 August 2016.
Published online 15 August 2016.

1. Manz, M. G. & Boettcher, S. Emergency granulopoiesis. *Nat. Rev. Immunol.* **14,** 302–314 (2014).
2. Ginhoux, F. & Jung, S. Monocytes and macrophages: developmental pathways and tissue homeostasis. *Nat. Rev. Immunol.* **14,** 392–404 (2014).
3. Heo, J. B. & Sung, S. Vernalization-mediated epigenetic silencing by a long intronic noncoding RNA. *Science* **331,** 76–79 (2011).
4. Xing, Z. *et al.* lncRNA directs cooperative epigenetic regulation downstream of chemokine signals. *Cell* **159,** 1110–1125 (2014).
5. Bouffi, C. *et al.* Transcription factor repertoire of homeostatic eosinophilopoiesis. *J. Immunol.* **195,** 2683–2695 (2015).
6. Luo, M. *et al.* Long non-coding RNAs control hematopoietic stem cell function. *Cell Stem Cell* **16,** 426–438 (2015).
7. Yona, S. *et al.* Fate mapping reveals origins and dynamics of monocytes and tissue macrophages under homeostasis. *Immunity* **38,** 79–91 (2013).
8. Geissmann, F. *et al.* Development of monocytes, macrophages, and dendritic cells. *Science* **327,** 656–661 (2010).
9. Dyer, K. D. *et al.* Functionally competent eosinophils differentiated ex vivo in high purity from normal mouse bone marrow. *J. Immunol.* **181,** 4004–4009 (2008).
10. Wang, K. C. *et al.* A long noncoding RNA maintains active chromatin to coordinate homeotic gene expression. *Nature* **472,** 120–124 (2011).
11. Zhang, H. *et al.* Long noncoding RNA-mediated intrachromosomal interactions promote imprinting at the Kcnq1 locus. *J. Cell Biol.* **204,** 61–75 (2014).
12. Wang, L. *et al.* LncRNA *Dum* interacts with Dnmts to regulate *Dppa2* expression during myogenic differentiation and muscle regeneration. *Cell Res.* **25,** 335–350 (2015).
13. Maass, P. G. *et al.* A misplaced lncRNA causes brachydactyly in humans. *J. Clin. Invest.* **122,** 3990–4002 (2012).
14. Villunger, A., Scott, C., Bouillet, P. & Strasser, A. Essential role for the BH3-only protein Bim but redundant roles for Bax, Bcl-2, and Bcl-w in the control of granulocyte survival. *Blood* **101,** 2393–2400 (2003).
15. Shinjyo, T. *et al.* Downregulation of Bim, a proapoptotic relative of Bcl-2, is a pivotal step in cytokine-initiated survival signaling in murine hematopoietic progenitors. *Mol. Cell. Biol.* **21,** 854–864 (2001).
16. Bouillet, P. *et al.* Proapoptotic Bcl-2 relative Bim required for certain apoptotic responses, leukocyte homeostasis, and to preclude autoimmunity. *Science* **286,** 1735–1738 (1999).
17. Simon, H.-U. *et al.* Refining the definition of hypereosinophilic syndrome. *J. Allergy Clin. Immunol.* **126,** 45–49 (2010).
18. Voigt, P., Tee, W.-W. & Reinberg, D. A double take on bivalent promoters. *Genes Dev.* **27,** 1318–1338 (2013).
19. Paschos, K., Parker, G. A., Watanatanasup, E., White, R. E. & Allday, M. J. BIM promoter directly targeted by EBNA3C in polycomb-mediated repression by EBV. *Nucleic Acids Res.* **40,** 7233–7246 (2012).
20. Zhao, J., Sun, B. K., Erwin, J. A., Song, J.-J. & Lee, J. T. Polycomb proteins targeted by a short repeat RNA to the mouse X chromosome. *Science* **322,** 750–756 (2008).
21. Rinn, J. L. *et al.* Functional demarcation of active and silent chromatin domains in human HOX loci by noncoding RNAs. *Cell* **129,** 1311–1323 (2007).
22. Kaneko, S. *et al.* Interactions between JARID2 and noncoding RNAs regulate PRC2 recruitment to chromatin. *Mol. Cell* **53,** 290–300 (2014).
23. Sarma, K. *et al.* ATRX directs binding of PRC2 to Xist RNA and Polycomb targets. *Cell* **159,** 869–883 (2014).
24. Csorba, T., Questa, J. I., Sun, Q. & Dean, C. Antisense COOLAIR mediates the coordinated switching of chromatin states at FLC during vernalization. *Proc. Natl Acad. Sci. USA* **111,** 16160–16165 (2014).
25. Ranzani, V. *et al.* The long intergenic noncoding RNA landscape of human lymphocytes highlights the regulation of T cell differentiation by linc-MAF-4. *Nat. Immunol.* **16,** 318–325 (2015).
26. Henao-Mejia, J.*et al.* Protocol for the generation of genetically modified mice using the CRISPR–Cas9 genome-editing system. *Cold Spring Harb. Protoc.* http://dx.doi.org/10.1101/pdb.prot090704 (2016).

Supplementary Information is available in the online version of the paper.

Acknowledgements We thank several of our colleagues for critically reading our manuscript and their suggestions. J.H.-M. was supported by the Children's Hospital of Philadelphia, the IFI and IDOM pilot projects, and the COE at the University of Pennsylvania (J.H.-M.); A.W. and R.A.F. by NIH NIAID 1R21AI110776-01; C.C.D.H. and R.A.F by Howard Hughes Medical Institute; J.J.K. by NIH NIDDK T32-DK00778017; S.P.S. by NIH NRSA F30-DK094708; W.K.M. by T32-AI05542803; A.R. and M.C.D. by New Innovator 1DP2OD008514, 1R33EB019767, NSF CAREER 1350601. This work was funded in part by the Division of Intramural Research, NIAID, NIH (M.A.M. and A.D.K.)

Author Contributions J.J.K., S.P.S., A.W., R.A.F. and J.H.-M. designed these experiments. J.J.K., S.P.S. and J.H.-M. wrote the manuscript. A.W. and R.A.F. edited the manuscript. L.G. and J.R. performed the bioinformatic analysis of lncRNA identification. J.S. and C.H. aided the generation novel mice. D.B.U.K. performed *in vitro* promoter targeting and eosinophil LNA transfection. M.A.C. and A.U. prepared and analysed the ChIP–seq and ATAC–seq. E.N.E. performed 3C. M.C.D. and A.R. performed FISH. M.A.M. and A.D.K. collected and aided in the analysis of HES patient samples. All other experiments and analyses were performed by J.J.K., S.P.S., S.J.M., J.H.-M. and A.W. with help from W.K.M., C.C.D.H., A.T.V., S.Z. and W.B.

Author Information ATAC–seq and ChIP–seq data have been deposited in the Gene Expression Omnibus under accession number GSE85073. Reprints and permissions information is available at www.nature.com/reprints. The authors declare no competing financial interests. Readers are welcome to comment on the online version of the paper. Correspondence and requests for materials should be addressed to A.W. (adam.williams@jax.org), R.A.F. (richard.flavell@yale.edu) or J.H.-M. (jhena@mail.med.upenn.edu).

Reviewer Information *Nature* thanks H. Y. Chang, S. Jung and the other anonymous reviewer(s) for their contribution to the peer review of this work.

METHODS

Mice. All mice were bred and maintained under pathogen-free conditions at an American Association for the Accreditation of Laboratory Animal Care accredited animal facility at the University of Pennsylvania or Yale University. Mice were housed in accordance with the procedures outlined in the Guide for the Care and Use of Laboratory Animals under an animal study proposal approved by an institutional Animal Care and Use Committee. Male and female mice between 4 and 12 weeks of age were used for all experiments. Littermate controls were used whenever possible.

C57BL/6 (wild type) and B6.SJL-Ptprc^{a} Pepc^{b}/Boy (B6.SJL) mice were purchased from The Jackson Laboratory. We generated *Morrbid*-deficient mice and the in *cis* and in *trans* double heterozygous mice (*Morrbid*$^{+/-}$, *Bcl2l11*$^{+/-}$) mice using the CRISPR/Cas9 system as previously described[26]. In brief, to generate *Morrbid*-deficient mice, single guide RNAs (sgRNAs) were designed against regions flanking the first and last exon of the *Morrbid* locus (Extended Data Fig. 1g). Cas9-mediated double-stranded DNA breaks resolved by non-homologous end joining (NHEJ) ablated the intervening sequences containing *Morrbid* in C57BL/6N one-cell embryos. The resulting founder mice were *Morrbid*$^{-/+}$, which were then bred to wild-type C57BL/6N and then intercrossed to obtain homozygous *Morrbid*-/- mice. One *Morrbid*-deficient line was generated. To control for potential off-target effects, mice were crossed for at least 5 generations to wild-type mice and then intercrossed to obtain homozygosity. Littermate controls were used when possible throughout all experiments.

To generate the in *cis* and in *trans* double heterozygous mice (*Morrbid*$^{+/-}$, *Bcl2l11*$^{+/-}$) mice, we first obtained mouse one-cell embryos from a mating between *Morrbid*$^{-/-}$ female mice and wild-type male mice. As such, the resulting one-cell embryos were heterozygous for *Morrbid* (*Morrbid*$^{+/-}$). We then micro-injected sgRNAs designed against intronic sequences flanking the second exon of *Bcl2l11*, which contains the translational start site/codon, into *Morrbid*$^{-/+}$ one-cell embryos (Extended Data Fig. 9). Cas9-mediated double-stranded DNA breaks resolved by NHEJ ablated the intervening sequences containing the second exon of *Bcl2l11* in *Morrbid*$^{+/-}$ (C57BL/6N) one-cell embryos, generating founder mice that were heterozygous for both *Bcl2l11* and *Morrbid* (*Bcl2l11*$^{+/-}$; *Morrbid*$^{-/+}$). Founder heterozygous mice were then bred to wild-type C57BL/6N to interrogate for the segregation of the *Morrbid*-deficient and *Bcl2l11*-defient alleles (Extended Data Fig. 9). Pups that segregated such alleles were named in *trans* and pups that did not segregate were labelled in *cis*. One line of in *cis* and in *trans* double heterozygous mice (*Bcl2l11*$^{+/-}$; *Morrbid*$^{-/+}$) lines were generated. To control for potential off-target effects, mice were crossed for at least 5 generations to wild-type (C57BL/6N) mice (for in *cis*) and to *Morrbid*$^{-/-}$ mice (for in *trans*) to maintain heterozygosity. To determine genetic rescue, samples from mice containing different permutations of *Morrbid* and *Bcl2l11* alleles (Fig. 4g–j) were analysed in a blinded manner by a single investigator not involved in the breeding or coding of these samples.

Flow cytometry staining, analysis and cell sorting. Cells were isolated from the indicated tissues (blood, spleen, bone marrow, peritoneal exudate, adipose tissue). Red blood cells were lysed with ACK. Single-cell suspensions were stained with CD16/32 and with indicated fluorochrome-conjugated antibodies. If run live, cells were stained with 7-AAD (7-amino-actinomycin D) to exclude non-viable cells. Otherwise, before fixation, Live/Dead Fixable Violet Cell Stain Kit (Invitrogen) was used to exclude non-viable cells. Active caspase staining using Z-VAD-FMK (CaspGLOW, eBiosciences) was performed according to the manufacturer's specifications. Apoptosis staining by annexin V+ (Annexin V Apoptosis Detection kit) was performed according to the manufacturer's recommendations. BrdU staining was performed using BrdU Staining Kit (eBioscience) according to the manufacturer's recommendations. For BCL2L11 staining, cells were fixed for 15 min in 2% formaldehyde solution, and permeabilized with flow cytometry buffer supplemented with 0.1% Triton X-100. All flow cytometry analysis and cell-sorting procedures were done at the University of Pennsylvania Flow Cytometry and Cell Sorting Facility using BD LSRII cell analysers and a BD FACSAria II sorter running FACSDiva software (BD Biosciences). FlowJo software (version 10 TreeStar) was used for data analysis and graphic rendering. All fluorochrome-conjugated antibodies used are listed in Supplementary Table 2.

Western blotting. 1×10^6 wild-type and *Morrbid*-deficient neutrophils sorted from mouse bone marrow were assayed for BCL2L11 protein expression by western blotting (Bim C34C5 rabbit monoclonal antibody, Cell Signaling), as previously described.

ChIP–qPCR. 2×10^6 wild-type and *Morrbid*-deficient neutrophils sorted from mouse bone marrow were cross-linked in a 1% formaldehyde solution for 5 min at room temperature while rotating. Crosslinking was stopped by adding glycine (0.2 M in 1 × PBS (phosphate buffered saline)) and incubating on ice for 2 min. Samples were spun at 2500*g* for 5 min at 4 °C and washed 4 times with 1 × PBS. The pellets were flash frozen and stored at −80 °C. Cells were lysed, and nuclei were isolated and sonicated for 8 min using a Covaris S220 (105 Watts, 2% duty cycle, 200 cycles per burst) to obtain approximately 200–500 bp chromatin fragments. Chromatin fragments were pre-cleared with protein G magnetic beads (New England BioLabs) and incubated with pre-bound anti-H3K27me3 (Qiagen), anti-EZH2 (eBiosciences), or mouse IgG1 (Santa Cruz Biotechnology) antibody-protein G magnetic beads overnight at 4 °C. Beads were washed once in low-salt buffer (20 mM Tris, pH 8.1, 2 mM EDTA, 50 mM NaCl, 1% Triton X-100, 0.1% SDS), twice in high-salt buffer (20 mM Tris, pH 8.1, 2 mM EDTA, 500 mM NaCl, 1% Triton X-100, 0.1% SDS), once in LiCl buffer (10 mM Tris, pH 8.1, 1 mM EDTA, 0.25 mM LiCl, 1% NP-40, 1% deoxycholic acid) and twice in TE buffer (10 mM Tris-HCl, pH 8. 0, 1 mM EDTA). Washed beads were eluted twice with 100 µl of elution buffer (1% SDS, 0.1 M $NaHCO_3$) and de-crosslinked (0.1 mg ml^{-1} RNase, 0.3 M NaCl and 0.3 mg ml^{-1} Proteinase K) overnight at 65 °C. The DNA samples were purified with Qiaquick PCR columns (Qiagen). qPCR was carried out on a ViiA7 Real-Time PCR System (ThermoFisher) using the SYBR Green detection system and indicated primers. Expression values of target loci were directly normalized to the indicated positive control loci, such as *MyoD1* for H3K27me3 and EZH2 ChIP analysis, and *Actb* for Pol II ChIP analysis. ChIP–qPCR primer sequences are listed in Supplementary Table 1.

ATAC–seq preparation, sequencing, and analysis. 50,000 wild-type and knockout cells, in triplicate, were spun at 500*g* for 5 min at 4 °C, washed once with 50 µl of cold 1× PBS and centrifuged in the same conditions. Cells were resuspended in 50 µl of ice-cold lysis buffer (10 mM Tris-HCl, pH7.4, 10 mM NaCl, 3 mM $MgCl_2$, 0.1% IGEPAL CA-630). Cells were immediately spun at 500*g* for 10 min at 4 °C. Lysis buffer was carefully pipetted away from the pellet, which was then resuspended in 50 µl of the transposition reaction mix (25 µl 2× TD buffer, 2.5 µl Tn5 Transposase (Illumina), 22.5 µl nuclease-free water) and then incubated at 37 °C for 30 min. DNA purification was performed using a Qiagen MinElute kit and eluted in 12 µl of Elution buffer (10 mM Tris buffer, pH 8.0). To amplify library fragments, 6 µl of the eluted DNA was mixed with NEBnext High-Fidelity 2× PCR Master Mix, 25 µM of customized Nextera PCR primers 1 and 2 (Supplementary Table 1), 100x SYBR Green I and used in PCR as follow: 72 °C for 5 min; 98 °C for 30 s; and thermocycling 4 times at 98 °C for 10 s; 63 °C for 30 s; 72 °C for 1 min. 5 µl of the 5 cycles PCR amplified DNA was used in a qPCR reaction to estimate the additional number of amplification cycles. Libraries were amplified for a total of 10–11 cycles and were then purified using a Qiagen PCR Cleanup kit and eluted in 30 µl of Elution buffer. The libraries were quantified using qPCR and bioanalyser data, and then normalized and pooled to 2 nM. Each 2 nM pool was then denatured with a 0.1 N NaOH solution in equal parts then further diluted to form a 20 pM denatured pool. This pool was then further diluted down to 1.8 pM for sequencing using the NextSeq500 machine on V2 chemistry and sequenced on a 1 × 75 bp Illumina NextSeq flow cell.

ATAC sequencing cells was done on Illumina NextSeq at a sequencing depth of ~40–60 million reads per sample. Libraries were prepared in triplicates. Raw reads were deposited under GSE85073. 2 × 75 bp paired-end reads were mapped to the mouse mm9 genome using 'bwa' algorithm with 'mem' option. Only reads that uniquely mapped to the genome were used in subsequent analysis. Duplicate reads were eliminated to avoid potential PCR amplification artifacts and to eliminate the high numbers of mtDNA duplicates observed in ATAC–seq libraries. Post-alignment filtering resulted in ~26–40 million uniquely aligned singleton reads per library and the technical replicates were merged into one alignment BAM file to increase the power of open chromatin signal in downstream analysis. Depicted tracks were normalized to total read depth. ATAC–seq enriched regions (peaks) in each sample was identified using MACS2 using the below settings:

MACS2-2.1.0.20140616/bin/macs2 callpeak -t <input tag file> -f BED -n <output peak file> -g 'mm' --nomodel --shift -100 --extsize 200 -B --broad

ChIP–seq preparation, sequencing and analysis. 10×10^6 wild-type and knockout mice neutrophils were cross-linked in a 1% formaldehyde solution for 10 min at room temperature while rotating. Crosslinking was stopped by adding glycine (0.2 M in 1 × PBS) and incubating on ice for 2 min. Samples were spun at 2500*g* for 5 min at 4 °C and washed 4 times with 1× PBS. The pellets were flash frozen and stored at −80 °C. Cells were lysed and sonicated (Branson Sonifier 250) for 9 cycles (30% amplitude; time, 20 s on, 1 min off). Lysates were spun at 18,400*g* for 10 min at 4 °C and resuspended in 3 ml of lysis buffer. A sample of 100 µl was kept aside as input and the rest of the samples were divided by the number of antibodies to test. Chromatin immunoprecipitation was performed with 10 µg of antibody-bound beads (anti-H3K27ac, H3K4me3, H3K4me1, H3K36me3 (Abcam) and anti-rabbit IgG (Santa Cruz), Dynal Protein G magnetic beads (Invitrogen)) and incubated overnight at 4 °C. Bead-bound DNA was washed, reverse cross-linked and eluted overnight at 65 °C, shaking at 950 r.p.m. Beads were removed using a magnetic stand and eluted DNA was treated with RNase A (0.2 µg µl^{-1}) for 1 h at 37 °C shaking at 950 r.p.m., then with proteinase K (0.2 µg µl^{-1}) for 2 h at 55 °C. 30 µg of glycogen (Roche) and 5 M of NaCl were adding to the samples. DNA was extracted with 1 volume of phenol:chlorofrom:isoamyl alcohol

and washed out with 100% ethanol. Dried DNA pellets were resuspended in 30 µl of 10 mM Tris HCl, pH 8.0, and DNA concentrations were quantified using Qubit. Starting with 10 ng of DNA, ChIP–seq libraries were prepared using the KAPA Hyper Prep Kit (Kapa Biosystems, Inc.) with 10 cycles of PCR. The libraries were quantified using qPCR and bioanalyser data then normalized and pooled to 2 nM. Each 2 nM pool was then denatured with a 0.1 N NaOH solution in equal parts then further diluted to form a 20 pM denatured pool. This pool was then further diluted down to 1.8 pM for sequencing using the NextSeq500 machine on V2 chemistry and sequenced on a 1 × 75 bp Illumina NextSeq flow cell.

ChIP sequencing was done on an Illumina NextSeq at a sequencing depth of ~30–40 million reads per sample. Raw reads were deposited under GSE85073. 75 bp single-end reads were mapped to the mouse mm9 genome using 'bowtie2' algorithm. Duplicate reads were eliminated to avoid potential PCR amplification artifacts and only reads that uniquely mapped to the genome were used in subsequent analysis. Depicted tracks were normalized to control IgG input sample. ChIP–seq-enriched regions (peaks) in each sample was identified using MACS2 using the below settings:

MACS2-2.1.0.20140616/bin/macs2 callpeak -t <ChIP tag file> -c <control tag file> -f BED -g 'mm' --nomodel –extsize=250 --bdg –-broad -n <output peak file>

RIP–qPCR. 10^7 immortalized BMDMs were collected by trypsinization and resuspended in 2 ml PBS, 2 ml nuclear isolation buffer (1.28 M sucrose; 40 mM Tris-HCl, pH 7.5; 20 mM $MgCl_2$; 4% Triton X-100), and 6 ml water on ice for 20 min (with frequent mixing). Nuclei were pelleted by centrifugation at 2,500*g* for 15 min. Nuclear pellets were resuspended in 1 ml RNA immunoprecipitation (RIP) buffer (150 mM KCl, 25 mM Tris, pH 7.4, 5 mM EDTA, 0.5 mM DTT, 0.5% NP40; 100 U ml^{-1} SUPERaseIn, Ambion; complete EDTA-free protease inhibitor, Sigma). Resuspended nuclei were split into two fractions of 500 µl each (for mock and immunoprecipitation) and were mechanically sheared using a dounce homogenizer. Nuclear membrane and debris were pelleted by centrifugation at 15,800*g*. for 10 min. Antibody to EZH2 (Cell Signaling 4905S; 1:30) or normal rabbit IgG (mock immunoprecipitation, SantaCruz; 10 µg) were added to supernatant and incubated for 2 hours at 4 °C with gentle rotation. 25 µl of protein G beads (New England BioLabs S1430S) were added and incubated for 1 hour at 4 °C with gentle rotation. Beads were pelleted by magnetic field, the supernatant was removed, and beads were resuspended in 500 µl RIP buffer and repeated for a total of three RIP buffer washes, followed by one wash in PBS. Beads were resuspended in 1 ml of Trizol. Co-precipitated RNAs were isolated, reverse-transcribed to cDNA, and assayed by qPCR for the *Hprt* and *Morrbid*-isoform1. Primer sequences are listed in Supplementary Table 1.

PAR–CLIP analysis. EZH2 PAR–CLIP dataset (GSE49435) was analysed as previously described[22]. Adapter sequences were removed from total reads and those longer than 17 bp were kept. The Fastx toolkit was used to remove duplicate sequences, and the resulting reads were mapped using BOWTIE allowing for two mismatches. The four independent replicates were pooled and analysed using PARalyzer, requiring at least two T→C conversions per RNA–protein contact site. lncRNAs were annotated according to Ensemble release 67.

Chromosome conformation capture (3C). 13×10^6 wild-type bone marrow derived mouse eosinophils were fixed with 1% formaldehyde for 10 minutes at room temperature, and quenched with 0.2 M glycine on ice. Eosinophils were lysed for 3–4 hours at 4 °C (50 mM Tris, pH 7.4, 150 mM NaCl, 0.5% NP-40, 1% Triton X-100, 1× Roche complete protease inhibitor) and dounce-homogenized. Lysis was monitored by Methyl-green pyronin staining (Sigma). Nuclei were pelleted and resuspended in 500 µl 1.4× NEB3.1 buffer, treated with 0.3% SDS for one hour at 37 °C, and 2% Triton X-100 for another hour at 37 °C. Nuclei were digested with 800 units BglII (NEB) for 22 hours at 37 °C, and treated with 1.6% SDS for 25 minutes at 65 °C to inactivate the enzyme. Digested nuclei were suspended in 6.125 ml of 1.25× ligation buffer (NEB), and were treated with 1% Triton X-100 for one hour at 37 °C. Ligation was performed with 1,000 units T4 DNA ligase (NEB) for 18 hours at 16 °C, and crosslinks were reversed by proteinase K digestion (300 µg) overnight at 65 °C. The 3C template was treated with RNase A (300 µg), and purified by phenol-chloroform extraction. Digested and undigested DNA were run on a 0.8% agarose gel to confirm digestion. To control for PCR efficiency, two bacterial artificial chromosomes (BACs) spanning the region of interest were combined in equimolar quantities and digested with 500 units BglII at 37 °C overnight. Digested BACs were ligated with 100 units T4 Ligase HC (Promega) in 60 µl overnight at 16 °C. Both BAC and 3C ligation products were amplified by qPCR (Applied Biosystems ViiA7) using SYBR fast master mix (KAPA biosystems). Products were run side by side on a 2% gel, and images were quantified using ImageJ. Intensity of 3C ligation products was normalized to intensity of respective BAC PCR product.

***Listeria monocytogenes* infections.** Mice were infected with 30,000 CFUs of *Listeria monocytogenes* (strain 10403s, obtained as a gift from E. J. Wherry) intravenously (i.v.). Mice were weighed and inspected daily. Mice were analysed at day 4 of infection to determine the CFUs of *L. monocytogenes* present in the spleen and liver.

Papain challenge. Papain was purchased from Sigma Aldrich and resuspended in at 1 mg ml^{-1} in PBS. Mice were intranasally challenged with 5 doses of 20 µg papain in 20 µl of PBS or PBS alone every 24 hours. Mice were killed 12 hours after the last challenge. Bronchoalveolar lavage was collected in two 1 ml lavages of PBS. Cellular lung infiltrates were collected after 1 hour digestion in RPMI supplemented with 5% FCS, 1 mg ml^{-1} collagenase D (Roche) and 10 µg ml^{-1} DNase I (Invitrogen) at 37 °C. Homogenates were passed through a cell strainer and infiltrates separated with a 27.5%, Optiprep gradient (Axis-Shield) by centrifugation at 1,175*g* for 20 min. Cells were removed from the interface and treated with ACK lysis buffer.

Bone marrow chimaeras. Congenic C57BL/6 (wild-type) bone marrow expressing CD45.1 and CD45.2 and *Morrbid*-deficient bone marrow expression CD45.2 was mixed in a 1:1 ratio and injected into C57BL/6 hosts irradiated twice with 5 Gy 3 hours apart that express CD45.1 (B6.SJL-Ptprc^a Pepc^b/BoyJ). Mice were analysed between 4–9 weeks after injection.

Bone-marrow-derived eosinophils. Bone marrow was isolated and cultured as previously described[9]. Briefly, unfractionated bone marrow cells were cultured with 100 ng ml^{-1} stem cell factor (SCF) and 100 ng ml^{-1} FLT3-ligand (FLT3-L). At day 4, the media was replaced with media containing 10 ng ml^{-1} interleukin (IL-5). Mature bone-marrow-derived eosinophils were analysed between day 10–14.

Bone-marrow-derived macrophage cultures. Bone marrow cells were isolated and cultured in media containing recombinant mouse M-CSF (10 ng ml^{-1}) for 7–8 days. On day 7–8, cells were re-plated for use in experimental assays. Bone-marrow-derived macrophages were stimulated with LPS (250 ng ml^{-1}) for the indicated periods of time.

ChIRP–qPCR. Briefly, 40×10^7 Immortalized bone-marrow-derived macrophages were fixed with 40 ml of 1% glutaraldehyde for 10 min at room temperature. Crosslinking was quenched with 0.125 M glycine for 5 min. Cells were rinsed with PBS, pelleted for 4 min at 2,000*g*, snap-frozen in liquid nitrogen, and stored at −80 °C. Cell pellets were thawed at room temperature and resuspended in 800 µl of lysis buffer (50 mM Tris-HCl, pH 7.0, 10 mM EDTA, 1% SDS, 1 mM PMSF, complete protease inhibitor (Roche), 0.1 U ml^{-1} Superase In (Life Technologies)). Cell suspension was sonicated using a Covaris S220 machine (Covaris; 100 W, duty factor 20%, 200 cycles per burst) for 60 minutes until DNA was in the size range of 100–500 bp. After centrifugation for 5 min at 16100 g at 4 °C, the supernatant was aliquoted, snap-frozen in liquid nitrogen, and stored at −80 °C. 1 ml of chromatin was diluted in 2 ml hybridization buffer (750 mM NaCl, 1% SDS, 50 mM Tris HCl, pH 7.0, 1 mM EDTA, 15% formamide) and input RNA and DNA aliquots were removed. 100 pmoles of probes (Supplementary Table 1) were added and mixed by rotation at 37 °C for 4 h. Streptavidin paramagnetic C1 beads (Invitrogen) were equilibrated with lysis buffer. 100 µl washed C1 beads were added, and the entire reaction was mixed for 30 min at 37 °C. Samples were washed five times with 1 ml of washing buffer (SSC 2×, 0.5% SDS and fresh PMSF). 10% of each sample was removed from the last wash for RNA isolation. RNA aliquots were added to 85 µl RNA PK buffer, pH 7.0, (100 mM NaCl, 10 mM TrisCl, pH 7.0, 1 mM EDTA, 0.5% SDS, 0.2 U $µl^{-1}$ proteinase K) and incubated for 45 min with end-to-end shaking. Samples were spun down, and boiled for 10 min at 95 °C. Samples were chilled on ice, added to 500 µl TRizol, and RNA was extracted according to the manufacturer's recommendations. Equal volume of RNA was reverse-transcribed and assayed by qPCR using *Hprt* and *Morrbid*-exon1-1 primer sets (Supplementary Table 1). DNA was eluted from remaining bead fraction twice using 150 µl DNA elution buffer (50 mM $NaHCO_3$, 1%SDS, 200 mM NaCl, 100 µg ml^{-1} RNase A, 100 U ml^{-1} RNase H) incubated for 30 min at 37 °C. DNA elutions were combined and treated with 15 µl (20 mg ml^{-1}) Proteinase K for 45 min at 50 °C. DNA was purified using phenol: chloroform:isoamyl and assayed by qPCR using the indicated primer sequences (Supplementary Table 1).

shRNA generation and transduction. shRNAs of indicated sequences (Supplementary Table 1) were cloned into pGreen shRNA cloning and expression lentivector. Psuedotyped lentivirus was generated as previously described, and 293T cells were transfected with a packaging plasmid, envelop plasmid, and the generated shRNA vector plasmid using Lipofectamine 2000. Virus was collected 14–16 h and 48 h after transfection, combined, 0.4-µm filtered, and stored at −80 °C. For generation of *in vivo* BM chimaeras, virus was concentrated 6 times by ultracentrifugation using an Optiprep gradient (Axis-Shield).

For transduced BM-derived eosinophils, cultured BM cells on day 3 of previously described culture conditions were mixed 1:1 with indicated lentivirus and spinfected for 2 h at 260*g* at 25 °C with 5 µg ml^{-1} polybrene. Cultures were incubated overnight at 37 °C, and media was exchanged for IL-5 containing media at day 4 of culture as previously described[9]. Cells were sorted for GFP^+ cells on day 5 of culture, and then cultured as previously described for eosinophil generation. Cells were assayed on day 11 of culture.

For transduced *in vivo* BM chimaeras, BM cells were cultured at 2.5×10^6 cells per ml in mIL-3 (10 ng ml^{-1}), mIL-6 (5 ng ml^{-1}) and mSCF (100 ng ml^{-1}) overnight at 37 °C. Culture was readjusted to 2 ml at 2.5×10^6 cells per ml in a 6-well

plate, and spinfected for 2 h at 260*g* at 25 °C with 5 μg ml^{-1} polybrene. Cells were incubated overnight at 37 °C. On the day before transfer, recipient hosts were irradiated twice with 5 Gy 3 hours apart. Mice were analysed between 4 and 5 weeks following transfer.

Locked nucleic acid knockdown. Bone marrow-derived macrophages (BMDMs) were transfected with pooled *Morrbid* or scrambled locked nucleic acid (LNA) antisense oligonucleotides of equivalent total concentrations using Lipofectamine 2000. *Morrbid* LNA pools contained *Morrbid* LNA 1-4 sequences at a total of 50 or 100 nM (Supplementary Table 1). After 24 h, the transfection media was replaced. The BMDMs were incubated for an additional 24 h and subsequently stimulated with LPS (250 ng ml^{-1}) for 8–12 h.

Eosinophils were derived from mouse BM as previously described. On day 12 of culture, 1×10^6 to 2×10^6 eosinophils were transfected with 50 nm of *Morrbid* LNA 3 or scrambled LNA (Supplementary Table 1) using TransIT-oligo according to manufacturer's protocol. RNA was extracted 48 h after transfection.

***Morrbid* promoter deletion.** Guide RNAs (gRNAs) targeting the 5' and 3' flanking regions of the *Morrbid* promoter were cloned into Cas9 vectors pSPCas9(BB)-2A-GFP(PX458) (Addgene plasmid 48138) and pSPCas9(BB)-2A-mCherry (a gift from the Stitzel lab, JAX-GM) respectively. gRNA sequences are listed in Supplementary Table 1. The cloned Cas9 plasmids were then transfected into RAW 264.7, a mouse macrophage cell line using Lipofectamine 2000, according to manufacturer's protocol. Forty–eight hours post transfection the double positive cells expressing GFP and mcherry, and the double negative cells lacking GFP and mcherry were sorted. The bulk sorted cells were grown in a complete media containing 20% FBS, assayed for deletion by PCR, as well as for *Morrbid* and *Bcl2l11* transcript expression by qPCR.

***Ex vivo* cytokine stimulation.** BM-derived eosinophils, or neutrophils or Ly6C^{hi} monocytes sorted from mouse BM, were rested for 4–6 hours at 37 °C in complete media. Cells were subsequently stimulated with IL-3 (10 ng ml^{-1}, Biolegend), IL-5 (10 ng ml^{-1}, Biolegend), GM-CSF (10 ng ml^{-1}, Biolegend), or G-CSF (10 ng ml^{-1}, Biolegend) for 4–6 h. RNA was collected at each time-point using TRIzol (Life Technologies).

GSK126 treatment. Wild-type and *Bcl2l11*$^{-/-}$ BM-derived eosinophils were generated as previously described[9]. On day 8 of culture, the previously described IL-5 media was supplemented with the indicated concentrations of the EZH2-specific inhibitor GSK126 (Toronto Research Chemicals). Media was exchanged for fresh IL-5 GSK126 containing media every other day. Cells were assayed for numbers and cell death by flow cytometry every day for 6 days following GSK126 treatment.

RNA extraction, cDNA synthesis and quantitative RT-PCR. Total RNA was extracted from TRIzol (Life Technologies) according to the manufacturer's instructions. Gycogen (ThermoFisher Scientific) was used as a carrier. Isolated RNA was quantified by spectophotemetry, and RNA concentrations were normalized. cDNA was synthesized using SuperScript II Reverse Transcriptase (ThermoFisher Scientific) according to the manufacturer's instructions. Resulting cDNA was analysed by SYBR Green (KAPA SYBR Fast, KAPABiosystems) or Taqman-based (KAPA Probe Fast, KAPABiosystems) using indicated primers. Primer sequences are listed in Supplementary Table 1. All reactions were performed in duplicate using a CFX96 Touch instrument (BioRad) or ViiA7 Real-Time PCR instrument (ThermoFischer Scientific).

RNA-seq and conservation analysis. Reads generated from mouse (Gr1$^+$) granulocytes (previously published GSE53928), human neutrophils (previously published GSE70068), and bovine peripheral blood leukocytes (previously published GSE60265) were filtered, normalized, and aligned to the corresponding host genome. Reads mapping around the *Morrbid* locus were visualized. For visualization of the high level of *Morrbid* expression in short-lived myeloid cells, reads from sorted mouse eosinophils (previously published GSE69707), were filtered, aligned to mm9, normalized using RPKM, and gene expression was plotted in descending order. For each human sample corresponding to the indicated stimulation conditions, the number of reads mapping to the human *MORRBID* locus per total mapped reads was determined.

For conservation across species, the genomic loci and surrounding genomic regions for the species analysed were aligned with mVista and visualized using the rankVista display generated with mouse as the reference sequence. Green highlights annotated mouse exonic regions and corresponding regions in other indicated species.

RNA fluorescence *in situ* hybridization. Single molecule RNA fluorescence *in situ* hybridization (FISH) was performed as previously described. A pool of 44 oligonucleotides (Biosearch Technologies) were labelled with Atto647N (Atto-Tec). For validation purposes, we also labelled subsets consisting of odd and even numbered oligonucleotides with Atto647N and Atto700, respectively, and looked for colocalization of signal. We designed the oligonucleotides using the online Stellaris probe design software. Probe oligonucleotide sequences are listed in Supplementary Table 1. Thirty *Z*-sections with a 0.3-μm spacing were taken for each field of view. We acquired all images using a Nikon Ti-E widefield microscope with a 100× 1.4NA objective and a Pixis 1024BR cooled CCD camera. We counted the mRNA in each cell by using custom image processing scripts written in MATLAB.

Cell fractionation. For nuclear and cytoplasmic fractionation, 5×10^6 BMDMs were stimulated with 250 ng ml^{-1} LPS for 4 hours. Cells were collected and washed once with cold PBS. Cells were pelleted, resuspended in 100 μl cold NAR A buffer (10 mM HEPES, pH 7.9, 10 mM KCl, 0.1 mM EDTA, 1× complete EDTA-free protease inhibitor, Sigma; 1 mM DTT, 20 mM β-glycerophasphate, 0.1 U μl^{-1} SUPERaseIn, Life Technologies), and incubated at 4 °C for 20 min. 10 μl 1% NP-40 was added, and cells were incubated for 3 min at room temperature. Cells were vortexed for 30 seconds, and centrifuged at 3,400*g*. for 1.5 min at 4 °C. Supernatant was removed, centrifuged at full speed for 90 min at 4 °C, and remaining supernatant was added to 500 μl Trizol as the cytoplasmic fraction. The original pellet was washed 4 times in 100 μl NAR A with short spins of 6,800*g*. for 1 min. The pellet was resuspended in 50 μl NAR C (20 mM HEPES, pH 7.9, 400 mM NaCl, 1 mM EDTA, 1× complete EDTA-free protease inhibitor, Sigma, 1 mM DTT, 20mM β-glycerophasphate, 0.1 U μl^{-1} SUPERaseIn, Life Technologies). Cells were vortexed every 3 min for 10 s for a total of 20 min at 4 °C. The sample was centrifuged at maximum speed for 20 min at room temperature. Remaining supernatant was added to 500 μl Trizol as the nuclear fraction. Equivalent volumes of cytoplasmic and nuclear RNA were converted to cDNA using gene specific primers and Super Script II RT (Life Technologies). Fraction was assessed by qPCR for *Morrbid*-exon1-1 and other known cytoplasmic and nuclear transcripts. Primer sequences are listed in Supplementary Table 1.

For cytoplasmic, nuclear, and chromatin fractionation, cell fractions 5×10^6 to 10×10^6 immortalized macrophages were activated with 250 ng ml^{-1} LPS (Sigma) for 6 hours at 37 °C. Cells were washed 2× with PBS, and then resuspended in 380 μl ice-cold HLB (50 mM Tris-HCl, pH7.4, 50 mM NaCl, 3 mM $MgCl_2$, 0.5% NP-40, 10% glycerol), supplemented with 100 U SUPERase In RNase Inhibitor (Life Technologies). Cells were vortexed 30 s and incubated on ice for 30 min, followed by a final 30 s vortex and centrifugation at 4 °C for 5 min × 1000*g*. Supernatant was collected as the cytoplasmic fraction. Nuclear pellets were resuspended by vortexing in 380 μl ice-cold MWS (50 mM Tris-HCl, pH7.4, 4 mM EDTA, 0.3 M NaCl, 1 M urea, 1% NP-40) supplemented with 100 U SUPERase in RNase Inhibitor. Nuclei were lysed on ice for 10 min, vortexed for 30 s, and incubated on ice for 10 more min to complete lysis. Chromatin was pelleted by centrifugation at 4 °C for 5 min × 1000*g*. Supernatant was collected as the nucleoplasmic fraction. RNA was collected as described previously and cleaned up using the RNeasy kit (Qiagen). Equivalent volumes of cytoplasmic, nucleoplasmic, and chromatin-associated RNA were converted to cDNA using random hexamers and Super Script III RT (Life Technologies). Fraction was assessed by qPCR for *Morrbid*-exon1-2 and other known cytoplasmic and nuclear transcripts. Primer sequences are listed in Supplementary Table 1.

Copy number analysis. *Morrbid* cDNA was cloned into reference plasmid (pCDNA3.1) containing a T7 promoter. The plasmid was linearized and *Morrbid* RNA was *in vitro* transcribed using the MEGAshortscript T7 kit (Life Technologies), according to the manufacturer's recommendations, and purified using the MEGAclear kit (Life Technologies). RNA was quantified using spectrophotometry and serial dilutions of *Morrbid* RNA of calculated copy number were spiked into *Morrbid*-deficient RNA isolated from *Morrbid*-deficient mouse spleen. Samples were reverse transcribed in parallel with wild-type-sorted neutrophil RNA and B-cell RNA isolated from known cell number using gene-specific *Morrbid* primers, and the *Morrbid* standard curve and wild-type neutrophils and B cells were assayed using qPCR with *Morrbid*-exon 1 primer sets (Supplementary Table 1)

Bromodeoxyuridine incorporation assay. Cohorts of mice were given a total of 4 mg bromodeoxyuridine (BrdU; Sigma Aldrich) in 2 separate intraperitoneal (i.p.) injections 3 h apart and monitored over the subsequent 5 days, unless otherwise noted. For analysis cells were stained according to manufacturer protocol (BrdU Staining Kit, ebioscience; anti-BrdU, Biolgend). A one-phase exponential curve was fitted from the peak labelling frequency to 36 h after peak labelling within each genetic background, and the half-life was determined from this curve.

Human samples. *Human subject cohort 1.* Study subjects were recruited and consented in accordance with the University of Pennsylvania Institutional Review Board. Peripheral blood was separated by Ficoll–Paque density gradient centrifugation, and the mononuclear cell layer and erythrocyte/granulocyte pellet were isolated and stained for fluorescence-associated cell sorting as previously described. Neutrophils (live, CD16$^+$F4/80^{int}CD3$^-$CD14$^-$CD19$^-$), eosinophils (live, CD16$^-$F4/80^{hi}CD3$^-$CD14$^-$CD19$^-$), T cells (live, CD3$^+$CD16$^-$), monocytes (live, CD14$^+$CD3$^-$CD16$^-$CD56$^-$), natural killer (NK) cells (live, CD56$^+$CD3$^-$CD16$^-$CD14$^-$), B cells (live, CD19$^+$CD3$^-$CD16$^-$CD14$^-$CD56$^-$).

Human subject cohort 2. Samples from human subjects were collected on NIAID IRB-approved research protocols to study eosinophilic disorders (NCT00001406)

or to provide controls for in vitro research (NCT00090662). All participants gave written informed consent. Eosinophils were purified from peripheral blood by negative selection and frozen at –80 °C in TRIzol (Life Technologies). Purity was >97% as assessed by cytospin. RNA was purified according to the manufacturer's instructions. Expression analysis by qPCR was performed in a blinded manner by an individual not involved in sample collection or coding of these of these samples. Plasma IL-5 levels were measured by suspension array in multiplex (Millipore). The minimum detectable concentration was 0.1 pg ml^{-1}.

Cell lines. RAW 264.7 cells were obtained from ATCC and were not authenticated, but were tested for mycoplasma contamination biannually. Immortalized C57/B6 macrophages were obtained as a generous gift from I. Brodsky. These cells were not authenticated, but were tested for mycoplasma contamination biannually.

Statistics. Samples sizes were estimated based on our preliminary phenotyping of *Morrbid*-deficient mice. Preliminary cell number analysis of eosinophils, neutrophils, and $Ly6C^{hi}$ monocytes suggested that there were very large differences between wild-type and *Morrbid*-deficient samples, which would allow statistical interpretation with relatively small numbers and no statistical methods were used to predetermine sample size. No animals were excluded from analysis. All experimental and control mice and human samples were run in parallel to control for experimental variability. The experiments were not randomized. Experiments corresponding to Fig. 3g–i and Fig. 4g–j were performed and analysed in a single-blinded manner. All other experiments were not blinded to allocation during experiments and outcome assessment. Correlation was determined by calculating the Spearman correlation coefficient. Half-life was estimated by calculating the one-phase exponential decay constant from the peak of labelling frequency to 36 h after peak labelling. *P* values were calculated using a two-way *t*-test, Mann–Whitney *U*-test, one-way ANOVA with Tukey post-hoc analysis, Kaplan–Meier Mantel–Cox test, and false discovery rate (FDR) as indicated. FDR was calculated using trimmed mean of M-values (TMM)-normalized read counts and the DiffBind R package as described in Extended Data Fig. 7c, d. All error bars indicate mean plus and minus the standard error of mean (s.e.m.).

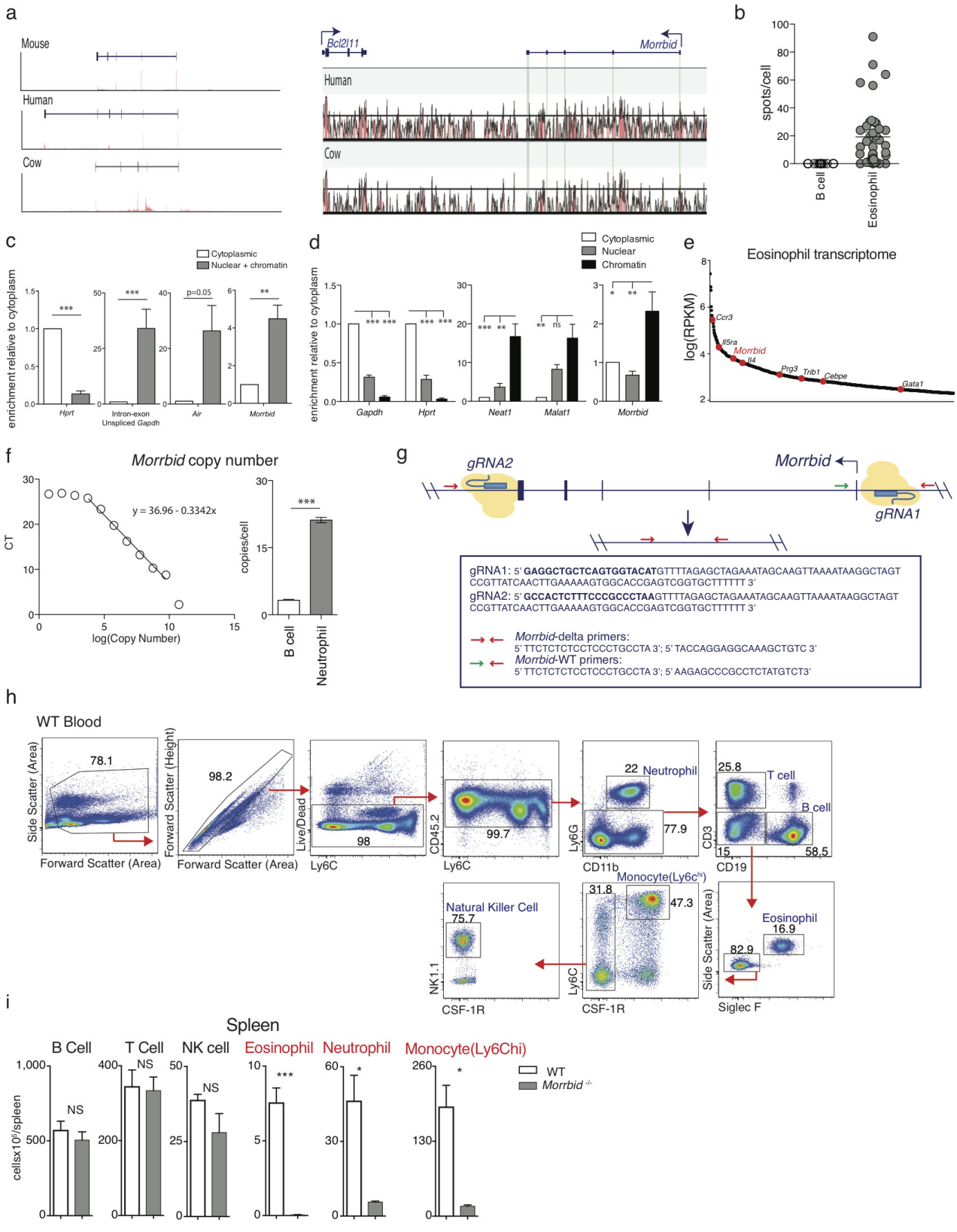

Extended Data Figure 1 | See next page for caption.

Extended Data Figure 1 | *Morrbid* transcript expression, localization, and conservation across species. a, Left: mouse, human and cow *Morrbid* transcripts. Human neutrophil, mouse granulocyte and cow peripheral blood RNA-seq data are represented as read density around the *Morrbid* transcript of each species. Right: the *Morrbid* loci and surrounding genomic regions of the indicated species were aligned with mVista and visualized using the rankVista display generated with mouse as the reference sequence. Green highlights annotated mouse exonic regions and corresponding regions in other indicated species. **b**, Quantification of *Morrbid* FISH spots per indicated cell population. Cells were stained with *Morrbid* RNA probes conjugated to 2 different fluorophores, and spots colocalizing in both fluorescent channels were quantified. **c**, Cytoplasmic and nuclear subcellular RNA fractionation of LPS-stimulated BMDMs with qPCR of indicated target transcripts ($n = 3$ macrophages generated from independent mice). **d**, Cytoplasmic, nuclear and chromatin subcellular RNA fractionation of LPS-stimulated immortalized BMDMs with qPCR of indicated target transcripts (average of 4 independent experiments). **e**, Mature eosinophil transcriptome sorted in descending order of log(RPKM) gene expression, with annotated select reported eosinophil-associated genes. **f**, Average number of *Morrbid* RNA copies per cell in sorted neutrophils and B cells. Left: standard curve generated using *in vitro* transcribed *Morrbid* RNA spiked into *Morrbid*-deficient RNA isolated from spleen. Right: calculated per cell *Morrbid* RNA copies ($n = 3$ replicates from independent mice). **g**, Representation of CRISPR–Cas9 targeting of the *Morrbid* locus with indicated guide RNA (gRNA) sequences and genotyping primer sets. Target gRNA sequences are bolded. **h**, Cells isolated from the blood of wild-type mice. Representative flow cytometry plots demonstrating the gating strategy for neutrophils ($CD45^+CD11b^+LY6G^+$), T cells ($CD45^+Ly6G^-CD3^+$), B cells ($CD45^+Ly6G^-CD3^-CD19+$), eosinophils ($CD45^+CD3^-CD19^-Ly6G^-SiglecF^+SSC^{hi}$), $Ly6C^{hi}$ monocytes ($CD45^+CD3^-CD19^-Ly6G^-SSC^{lo}SiglecF^-Ly6C^{hi}CSF\text{-}1R^+$), NK cells ($CD45^+CD3^-CD19^-Ly6G^-SSC^{lo}SiglecF^-CSF\text{-}1R^-NK1.1^+$). **i**, Total cell numbers of the indicated cell populations isolated from the spleen of wild-type and *Morrbid*-deficient mice ($n = 3$–5 mice per group, results representative of 8 independent experiments). Error bars show s.e.m. $^*P < 0.05$, $^{**}P < 0.01$, and $^{***}P < 0.001$ (two-sided *t*-test, **c**, **f**, **i**; one-way ANOVA with Tukey post-hoc analysis, **d**).

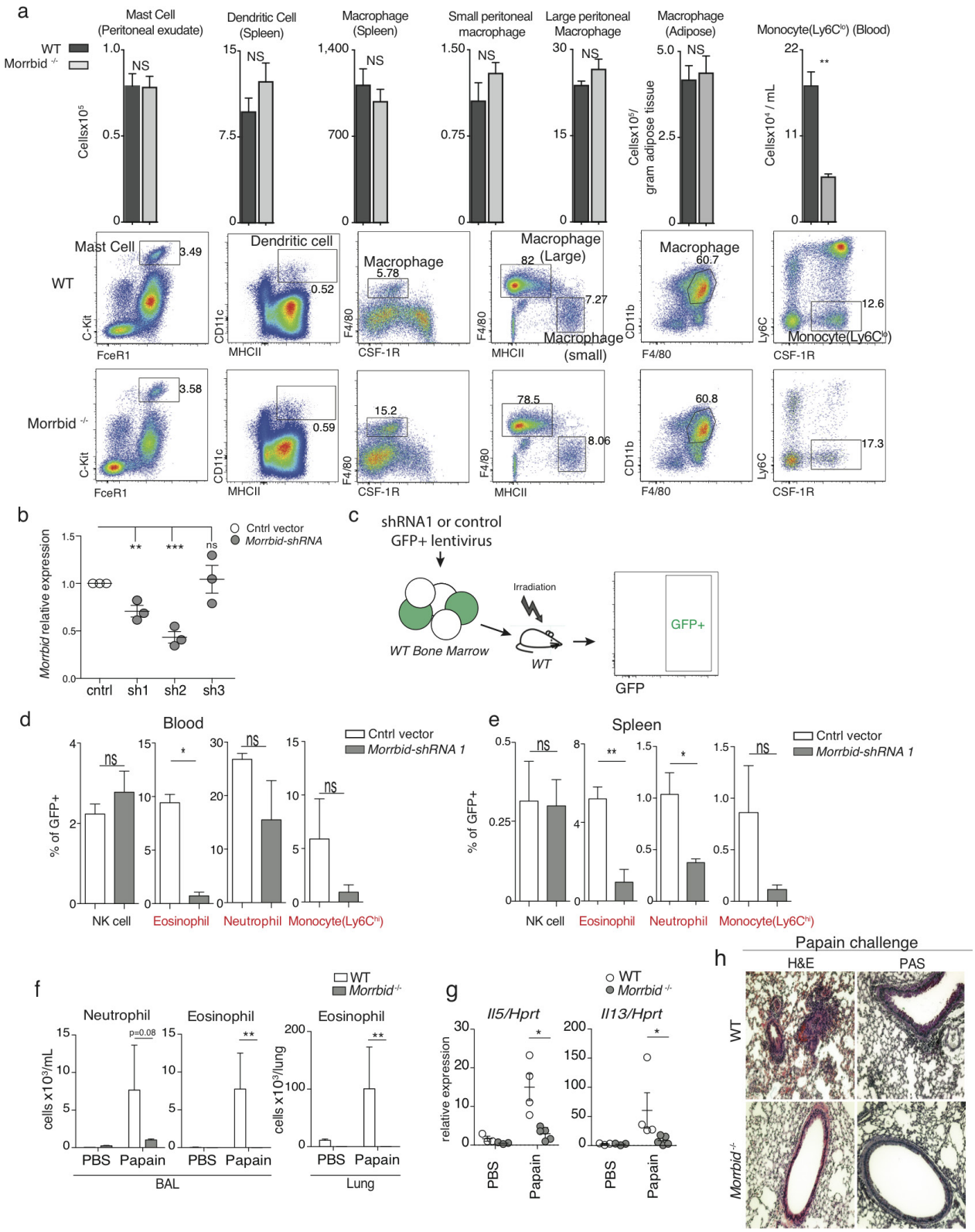

Extended Data Figure 2 | Myeloid cell populations in tissue following *Morrbid* deletion, and blood and spleen following *Morrbid* knockdown *in vivo*. **a**, Representative flow cytometry plots and absolute counts of the indicated cell populations in wild-type and *Morrbid*-deficient mice ($n = 3–5$ mice per group, representative of 3–7 independent experiments). **b**, shRNA knockdown of *Morrbid* RNA relative to control vector in BM-transduced with the indicated GFP vector, sorted on GFP, differentiated into eosinophils and assessed by qPCR (each dot represents eosinophils generated from independent mice). **c**, Schematic of control and *Morrbid* shRNA1 BM chimaera generation. **d**, **e**, Frequency of indicated cell populations within total GFP$^+$ transduced cells from blood (**d**) and spleen (**e**) ($n = 3–4$ mice per transduction group). **f**–**h**, Wild-type and *Morrbid*-deficient mice challenged with papain or PBS. **f**, Absolute numbers of indicated cell populations in lung tissue and broncholalveolar lavage (BAL). **g**, qPCR expression in lung tissue. **h**, Representative haematoxylin and eosin (H&E) and periodic acid–Schiff (PAS) stain lung histology at 40× magnification ($n = 3–4$ mice per group; representative of two independent experiments). Error bars show s.e.m. $^*P < 0.05$, $^{**}P < 0.01$, and $^{***}P < 0.001$ (two-sided *t*-test, **a**, **b**, **d**, **e**; Mann-Whitney *U*-test, **f**, **g**).

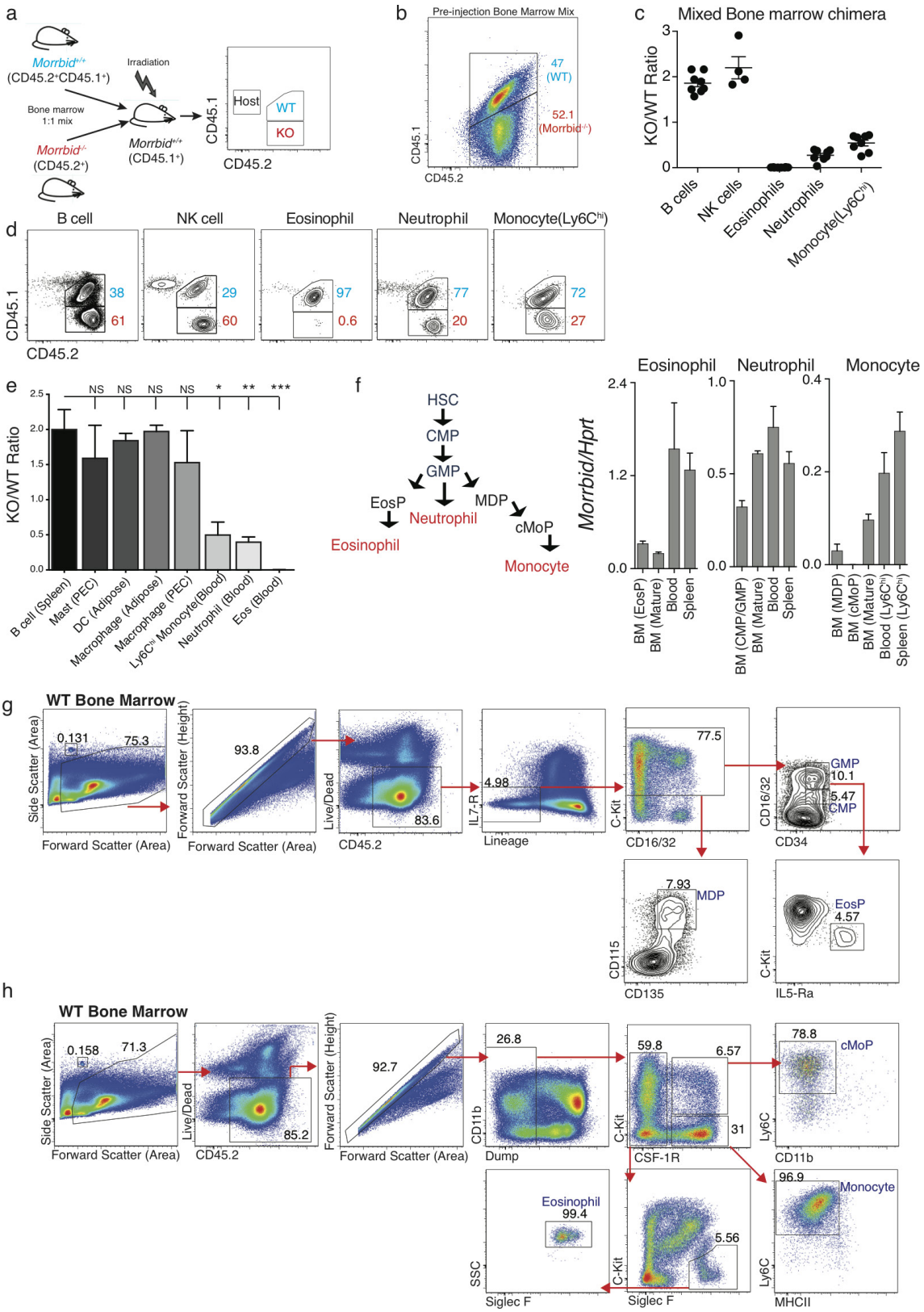

Extended Data Figure 3 | See next page for caption.

Extended Data Figure 3 | *Morrbid* regulation of mature neutrophils, eosinophils and Ly6C^{hi} monocytes is cell intrinsic. a–e, *Morrbid*-deficient competitive BM chimaera generation. **a**, Schematic of mixed BM chimaera generation. Congenically labelled wild-type CD45.1$^+$CD45.2$^+$ and *Morrbid*-deficient CD45.2$^+$ BM cells were mixed 1:1 and injected into an irradiated CD45.1$^+$ host. **b**, Ratio of mixed congenically labelled wild-type CD45.1$^+$CD45.2$^+$ and *Morrbid*-deficient CD45.2$^+$ BM cells before injection into an irradiated CD45.1$^+$ host. **c**, **d**, Ratio of *Morrbid*-deficient to wild-type short-lived myeloid and control immune cells in blood (**c**) and representative flow cytometry plots of these cell populations (**d**). **e**, *Morrbid*-deficient to wild type ratio of additional immune cell populations ($n = 4$–8 mice per group; pooled from two independent experiments). **f**, Schematic of myeloid differentiation and *Morrbid* qPCR expression in the indicated sorted progenitor and mature cells ($n = 3$–5 mice per group; representative of 3 independent experiments). **g**, Cells isolated from the BM of wild-type mice. Representative flow cytometry plots demonstrating the gating strategy for common myeloid progenitor (CMP): lineage (Sca1, CD11b, GR-1, CD3, Ter-119, CD19, B220, NK1.1), IL7Ra$^-$C-kit$^+$CD34$^+$CD16/32$^{lo/int}$; granulocyte/monocyte progenitor (GMP): lineage$^-$IL7Ra$^-$C-kit$^+$CD34$^+$CD16/32^{hi}; monocyte/dendritic cell progenitor (MDP): lineage$^-$IL7Ra$^-$C-kit$^+$CD115$^+$CD135$^+$; eosinophil progenitor (EosP): lineage$^-$IL7Ra$^-$C-kit$^+$CD34$^+$CD16/32^{hi}IL-5Ra$^+$. **h**, Cells isolated from the BM of wild-type mice. Representative flow cytometry plots demonstrating the gating strategy for eosinophils: dump$^-$ (dump: CD3, NKp46, Ter119, CD19, Ly6G, Sca1), CSF-1R$^-$C-kit$^{-/lo}$SiglecF$^+$ SSC^{hi}; monocytes: dump$^-$CSF-1R$^+$C-kit$^-$MHCII$^-$Ly6C^{hi}; common monocyte progenitor (cMoP): dump$^-$CSF-1R$^+$C-kit$^+$Ly6C^{hi}CD11b^{lo}. Flow cytometry count beads are visualized and gated by forward and side scatter area (**g**, **h**). Error bars show s.e.m. $^*P < 0.05$, $^{**}P < 0.01$, and $^{***}P < 0.001$ (one-way AVONA with Tukey post-hoc test analysis).

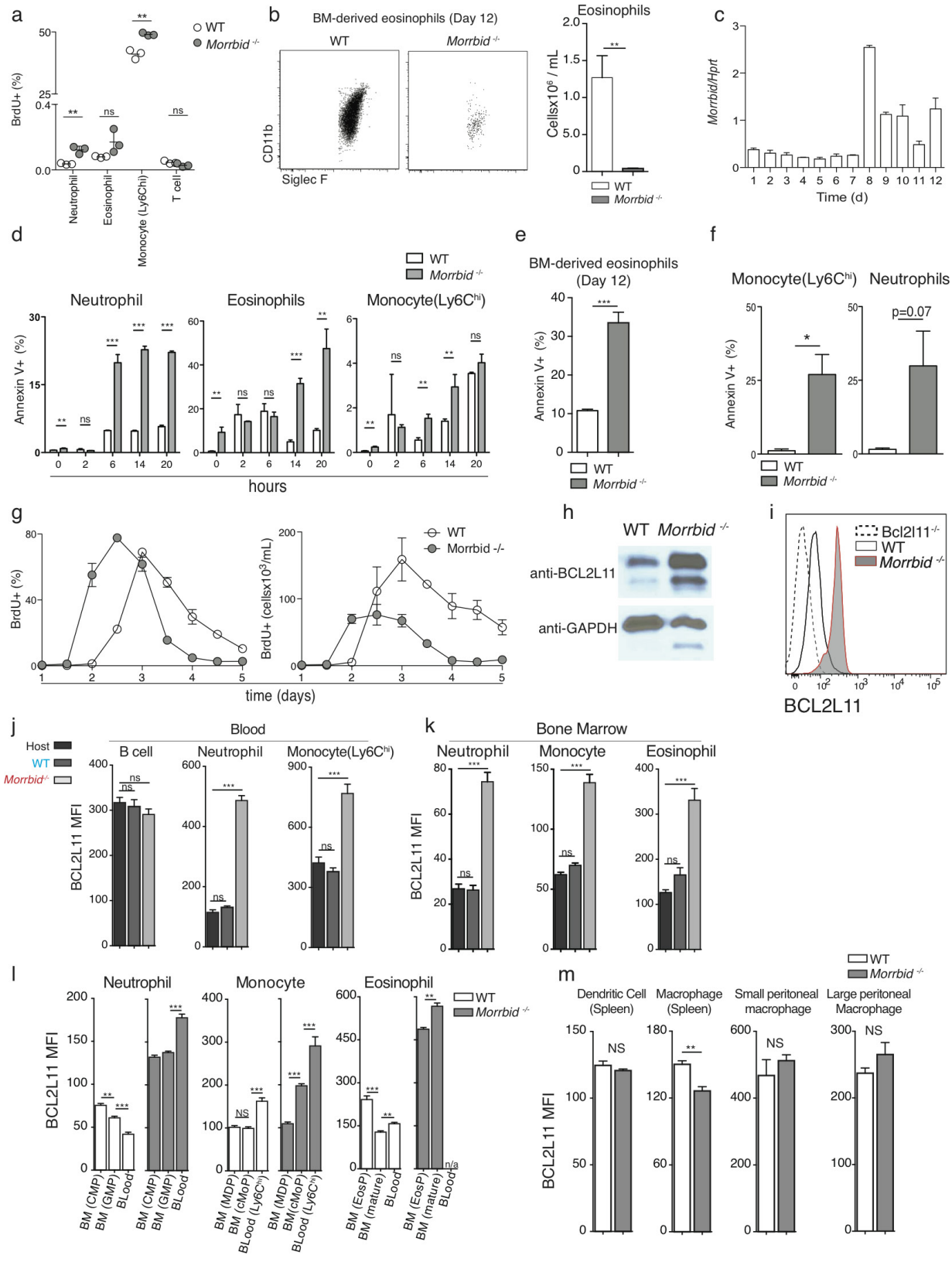

Extended Data Figure 4 | See next page for caption.

Extended Data Figure 4 | *Morrbid* regulates neutrophil, eosinophil and Ly6C^{hi} monocyte lifespan through cell-intrinsic regulation of *Bcl2l11*. **a**, Flow cytometric analysis of percentage of BrdU incorporation in the indicated wild-type and *Morrbid*-deficient immune cell populations from blood. Mice were analysed 24 h after one dose of 2 mg BrdU ($n = 3$ mice per group). **b**, Representative flow cytometry plots and absolute counts of mature eosinophils (live, CD45$^+$SSC^{hi}CD11b$^+$Siglec F$^+$) of BM-derived eosinophil culture on day 12 in wild-type and *Morrbid*-deficient mice ($n = 3$ mice per group, results representative of 3 independent experiments). **c**, *Morrbid* expression of developing wild-type BM-derived eosinophils at indicated time points of *in vitro* culture ($n = 3$ mice per group). **d**, Percentage of annexin V$^+$ wild-type and *Morrbid*-deficient BM cell populations at indicated time points of *ex vivo* culture ($n = 3$ mice per group; data are representative of two independent experiments). **e**, Percentage of annexin V$^+$ eosinophils (gated on annexin-V$^+$CD45$^+$SSC^{hi}CD11b$^+$SiglecF$^+$) of BM-derived eosinophil culture on day 12 in wild-type and *Morrbid*-deficient mice ($n = 3$ mice per group, results representative of 3 independent experiments). **f**, Percentage of annexin V$^+$ wild-type and *Morrbid*-deficient neutrophils and Ly6C^{hi} monocytes 4 days after *L. monocytogenes* infection ($n = 3$ mice per group, representative of 2 independent experiments). **g**, Flow cytometric analysis of percentage and absolute number of blood neutrophils from wild-type or *Morrbid*-deficient mice that were pulsed two times with 2 mg BrdU 3 h apart and monitored over 5 days ($n = 4$ mice per group; data are representative of three independent experiments). **h**, Western blot analysis of BCL2L11 protein expression in wild-type and *Morrbid*-deficient sorted BM neutrophils. **i**, BCL2L11 protein expression measured by flow cytometry in blood neutrophils from wild-type, *Morrbid*-deficient and *Bcl2l11*-deficient mice ($n = 1$–4 mice per group). **j**, **k**, BCL2L11 protein expression in mixed BM chimaera model. Quantification of mean fluorescence intensity (MFI) of BCL2L11 protein expression in indicated cell populations from blood (**j**) and BM (**k**) ($n = 4$–8 mice per group, results representative of two independent experiments). **l**, BCL2L11 protein expression in the indicated progenitors and mature cell types from wild-type and *Morrbid*-deficient mice. 'n/a' indicates that too few cells were present for MFI quantification ($n = 3$–5 mice per group, results representative of 3 independent experiments). **m**, BCL2L11 expression measured in the indicated cell populations from wild-type and *Morrbid*-deficient mice ($n = 3$, results representative of two independent experiments). Error bars show s.e.m. $^*P < 0.05$, $^{**}P < 0.01$, and $^{***}P < 0.001$ (two-sided *t*-test).

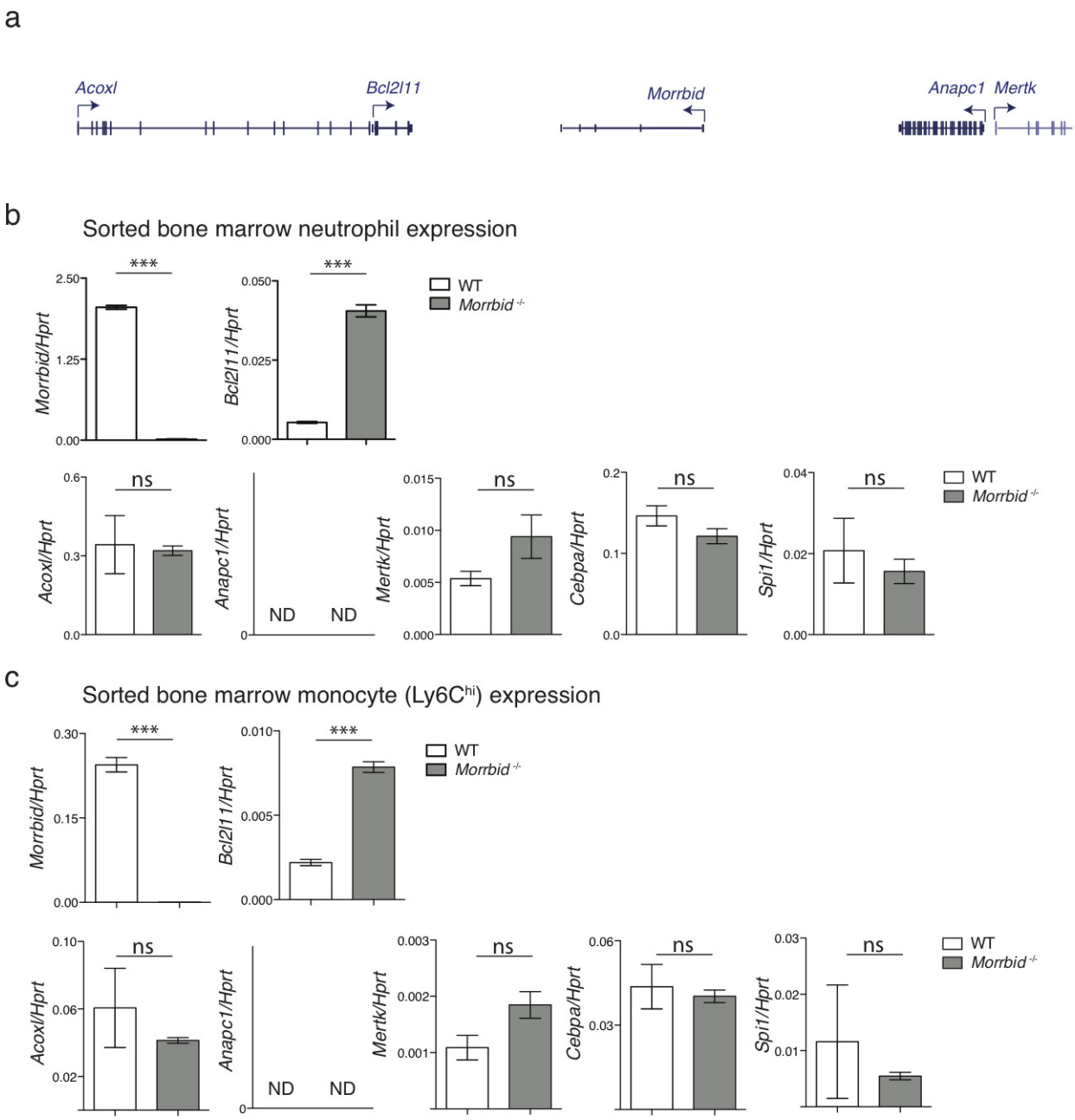

Extended Data Figure 5 | *Morrbid* specifically controls *Bcl2l11* expression. a, Schematic representation of genes surrounding the *Morrbid* locus. **b**, **c**, Expression of indicated transcripts assessed by qPCR in neutrophils (**b**) and Ly6C^{hi} (**c**) monocytes sorted from wild-type and *Morrbid*-deficient mice. ND (not detected) indicates expression was below the limit of detection ($n = 3$ mice per group, representative of 2 independent experiments). Error bars show s.e.m. $^{*}P < 0.05$, $^{**}P < 0.01$, and $^{***}P < 0.001$ (two-sided *t*-test).

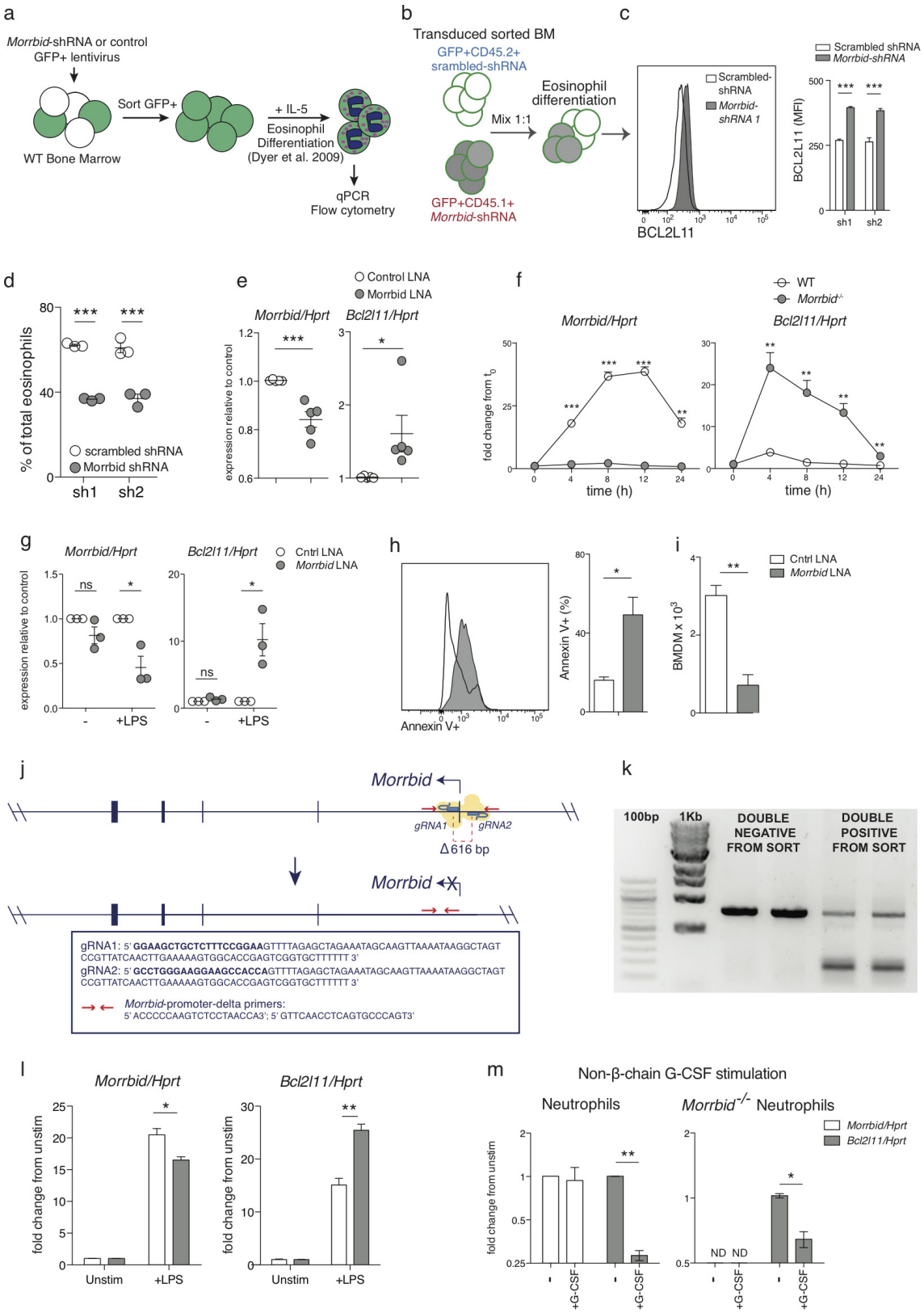

Extended Data Figure 6 | See next page for caption.

Extended Data Figure 6 | Knockdown of *Morrbid* leads to *Bcl2l11* upregulation and cell death. a, Schematic of shRNA-transduced BM-derived eosinophil system. **b**–**d**, *In vitro* shRNA BM-derived eosinophil competitive chimaera. **b**, Schematic of transduction of $CD45.2^+$ and $CD45.1^+$ BM cells transduced with GFP scrambled shRNA or GFP *Morrbid*-specific shRNA lentiviral vectors, respectively. GFP^+ cells were sorted, mixed 1:1, differentiated into eosinophils, and analysed by flow cytometry. **c**, Representative histogram and MFI quantification of BCL2L11 expression of mature eosinophils separated by congenic marker. **d**, Percentage of contribution of each congenic BM to the total mature eosinophil pool ($n = 3$ mice per group, each dot represents eosinophils differentiated from the BM of 1 mouse, representative of 2 independent experiments). **e**, *Morrbid* and *Bcl2l11* expression of wild-type BM-derived eosinophils transfected with *Morrbid*-specific LNA 3 and control LNA (each dot represents the average of 2–3 biological replicates, data pooled from 5 independent experiments). **f**, *Morrbid* and *Bcl2l11* expression of wild-type and *Morrbid*-deficient BM-derived macrophages at the indicated time points following LPS stimulation. Expression is represented as fold change from time 0 (t_0) ($n = 3$ mice per group, representative of 3 independent experiments). **g**–**i**, LPS-stimulated BM-derived macrophages transfected with pooled *Morrbid*-specific (LNA 1–4) or scrambled (cntrl LNA) antisense LNAs. **g**, *Morrbid* and *Bcl2l11* qPCR expression; **h**, Annexin V^+ expression; **i**, absolute BM-derived macrophage numbers ($n = 3$ mice per group, representative of 6 independent experiments). **j**–**l**, *Morrbid* promoter deletion in immortalized BMDMs. **j**, Diagram of *Morrbid* promoter targeting in immortalized BMDMs using CRISPR–Cas9. Immortalized BMDMs were transfected with GFP-expressing Cas9 and Cherry-expressing gRNA vectors of the indicated sequences. **k**, **l**, $GFP^+/Cherry^+$ and $GFP^-/Cherry^-$ expressing cells were sorted and assayed at the bulk level using PCR for verification of promoter deletion using the indicated primers (**j**, **k**) and qPCR for *Morrbid* and *Bcl2l11* expression following LPS stimulation for 6 hours (**l**) ($n = 3$ LPS-stimulated cultures, average of 3 independent experiments). **m**, *Morrbid* and *Bcl2l11* transcript expression in wild-type and *Morrbid*-deficient sorted BM-derived neutrophils stimulated with G-CSF for 4 h. Expression is represented as fold change from unstimulated ($n = 3$ mice, representative of 2 independent experiments). Error bars show s.e.m. $^*P < 0.05$, $^{**}P < 0.01$, and $^{***}P < 0.001$ (two-sided *t*-test).

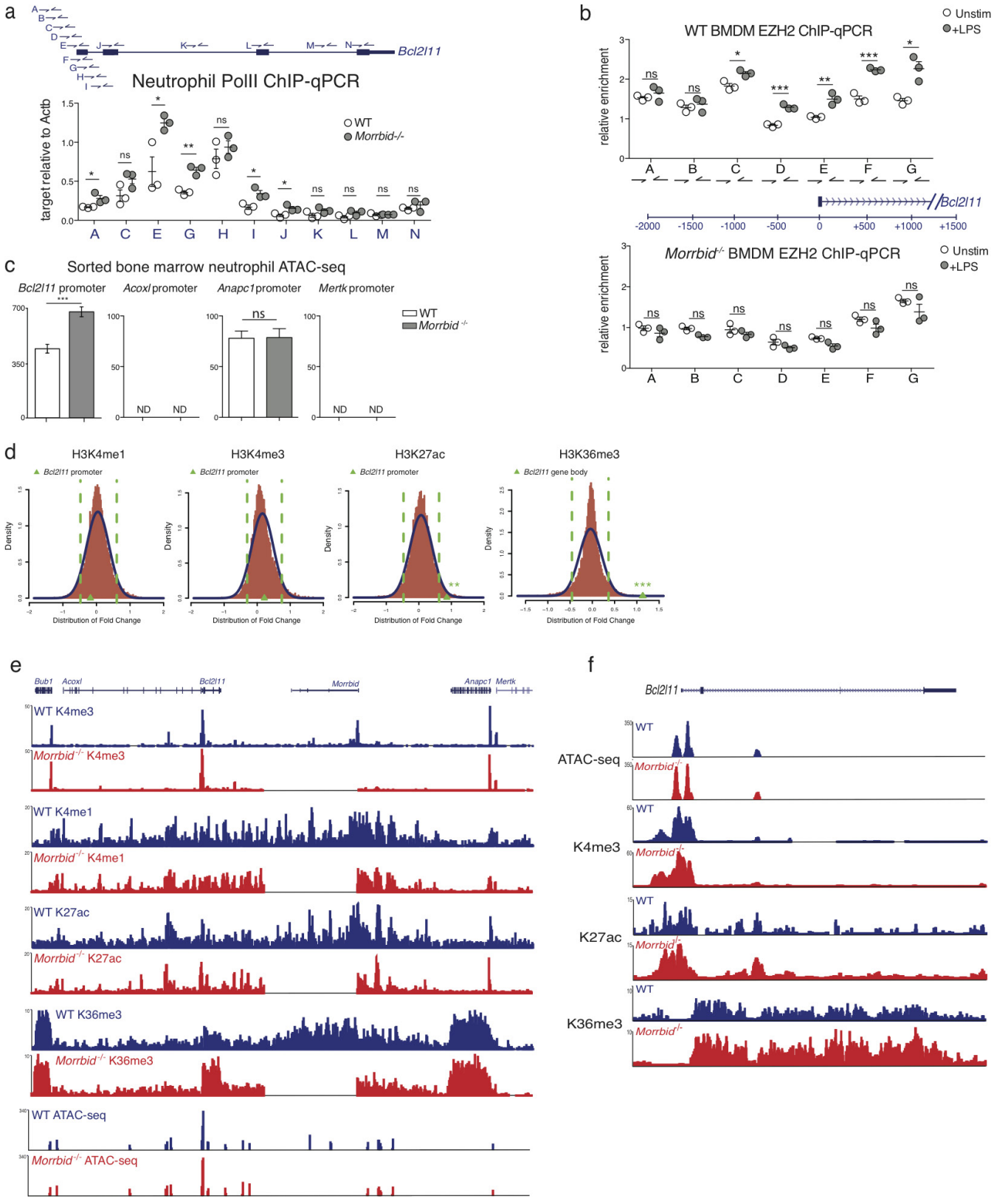

Extended Data Figure 7 | See next page for caption.

Extended Data Figure 7 | Epigenetic effect of *Morrbid* deletion on its surrounding genomic region. a, ChIP–qPCR analysis of total Pol II enrichment within the *Bcl2l11* promoter and gene body in wild-type and *Morrbid*-deficient neutrophils. Results are represented as *Bcl2l11* enrichment relative to control *Actb* enrichment within each sample. Each dot represents 1–2 pooled mice. **b**, ChIP–qPCR analysis of EZH2 enrichment within the *Bcl2l11* promoter in wild-type and *Morrbid*-deficient BMDMs stimulated with LPS for 12 hours. Results are represented as *Bcl2l11* enrichment relative to control *MyOD1* enrichment within each sample ($n = 3$, each dot represents BMDMs generated from 1 mouse). **c**, Relative chromatin accessibility levels at the *Bcl2l11*, *Acoxl*, *Anapc1* and *Mertk* promoters in *Morrbid*$^{-/-}$ and wild-type neutrophils as assessed by ATAC–seq. Chromatin accessibility levels were estimated as an average trimmed mean of M-values (TMM)-normalized read count across the replicates. Statistics were obtained by differential open chromatin analysis using the DiffBind R package. The *Bcl2l11* promoter is more open in *Morrbid*$^{-/-}$ neutrophils with a 1.52-fold change with a FDR of $< 0.1\%$. ND (not detected) indicates that no peak was present at the indicated promoter. **d**, Density plot of $\log_2$ fold-change distribution for H3K4me1, H3K4me3, H3K27ac and H3K36me3 levels between *Morrbid*$^{-/-}$ and wild-type neutrophils. Relative fold changes are estimated as the ratio of TMM-normalized read counts within consensus peak regions and were obtained using the DiffBind R package. Positive and negative fold changes indicate higher levels of ChIP binding in *Morrbid*$^{-/-}$ and wild-type neutrophils, respectively. Dashed green lines show the 5th and 95th percentiles. The green triangles on the *x* axis mark the change at the *Bcl2l11* promoter or gene body between wild-type and *Morrbid*$^{-/-}$ neutrophils. **e**, **f**, ATAC–seq and ChIP–seq for H3K4me1, H3K4me3, H3K27ac and H3K36me3 chromatin modifications were performed on neutrophils sorted from the bone marrow of wild-type and *Morrbid*-deficient mice. ATAC–seq and ChIP–seq are represented as read density surrounding the *Morrbid* locus (**e**) and at the *Bcl2l11* locus (**f**). ATAC–seq tracks are expressed as reads normalized to total reads, and chromatin modification tracks are expressed as reads normalized to input. Error bars show s.e.m. $^{*}P < 0.05$, $^{**}P < 0.01$, and $^{***}P < 0.001$ (two-sided *t*-test, **a**, **b**; FDR of fold change as described above, **c**, **d**).

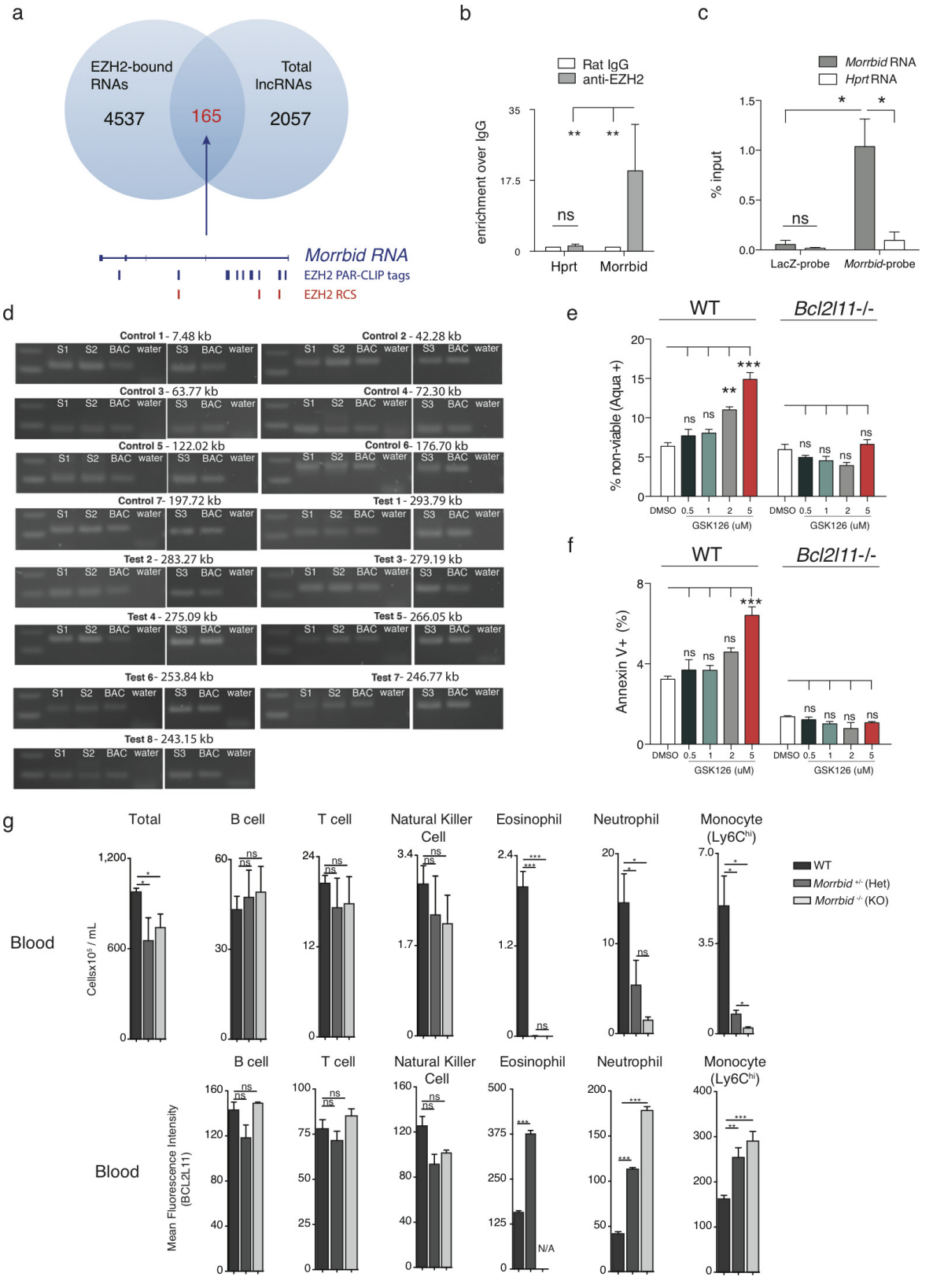

Extended Data Figure 8 | See next page for caption.

Extended Data Figure 8 | *Morrbid* represses *Bcl2l11* by maintaining its bivalent promoter in a poised state and phenotype of *Morrbid* heterozygous mice. a, Venn diagram summary of EZH2 PAR–CLIP analysis, with representation of tags and RNA–protein contact sites as determined by PARalyzer mapping to *Morrbid.* RNA contact sites (RCS) are displayed in red. **b**, Co-immunoprecipitation of the PRC2 family member EZH2 and *Morrbid*. Nuclear extracts of immortalized wild-type BMDMs stimulated with LPS for 6–12 h were immunoprecipitated by IgG or anti-EZH2 antibodies. Co-precipitation of indicated RNAs were assayed by qPCR. Data are represented as enrichment over IgG control ($n = 6$ biological replicates pooled from 2 independent experiments, representative of 3 independent experiments). **c**, Validation of *Morrbid* RNA pull-down over other RNAs using pools of *Morrbid* capture probes and LacZ probes ($n = 3$, average of 3 independent experiments). **d**, Visualized 3C PCR products from bait and indicated reverse primers using template from fixed and ligated BM-derived eosinophil DNA (S1, S2 and S3), BAC control (BAC) or water. The sequence of each reverse primer is listed in Supplementary Table 1. **e**, **f**, BM-derived eosinophils from wild-type and *Bcl2l11*$^{-/-}$ mice treated with EZH2 inhibitor GSK126 over time. Frequency of non-viable (Aqua^{+}) (**e**) and annexin V (**f**) staining cells on day 5 following treatment with GSK126 ($n = 3$ independently differentiated eosinophils per dose, results representative of 2 independent experiments). **g**, Total cell numbers (top) and BCL2L11 protein expression (bottom) of indicated cell populations from the blood of wild-type, *Morrbid*-heterozygous and *Morrbid*-deficient mice ($n = 3$–5 mice per group, results representative of 3 independent experiments). Error bars show s.e.m. $^{*}P < 0.05$, $^{**}P < 0.01$, and $^{***}P < 0.001$ (two-sided *t*-test, **c**, **g**; one-way ANOVA with Tukey post-hoc analysis, **e**, **f**; Mann–Whitney *U*-test, **b**).

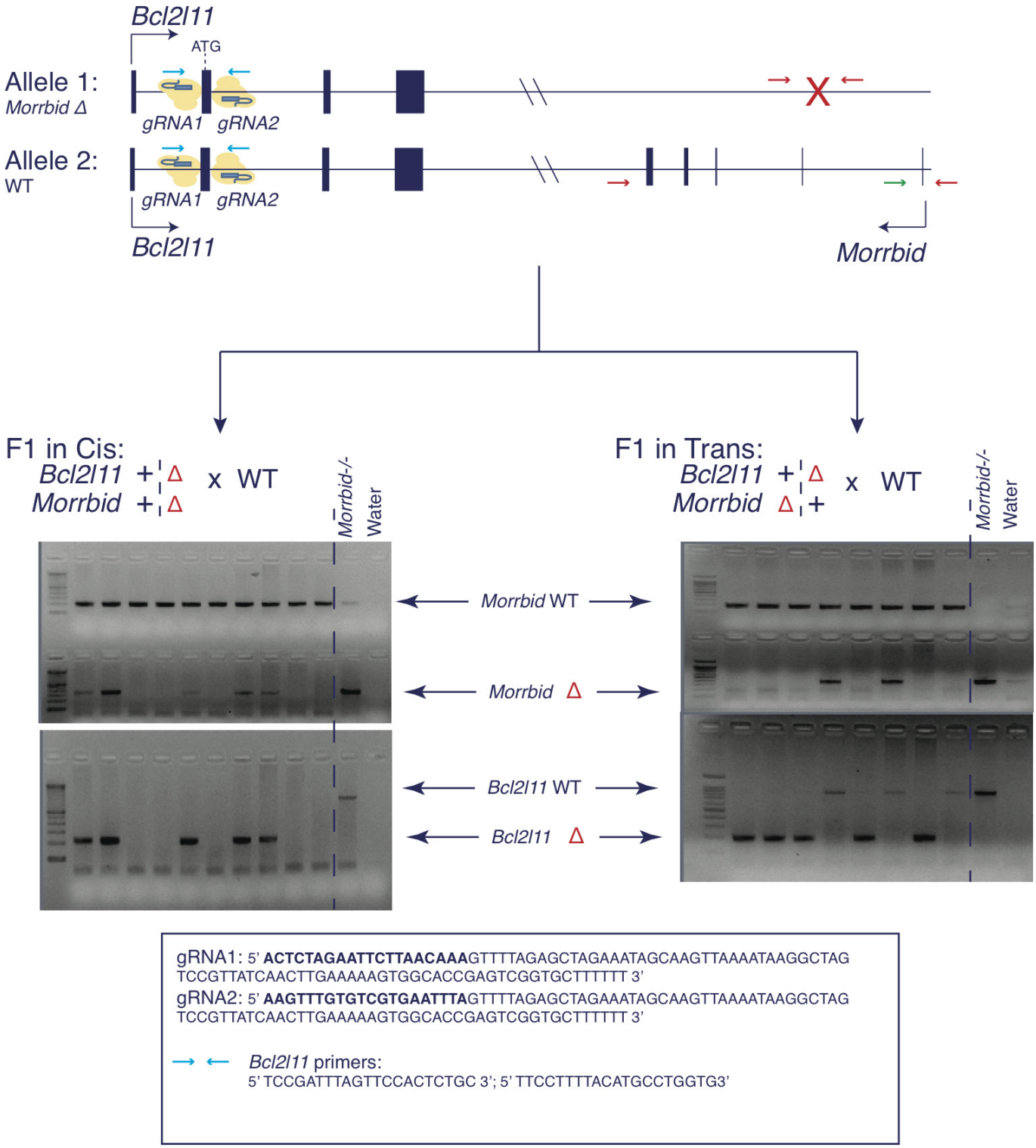

Extended Data Figure 9 | Generation of *Morrbid-Bcl2l11* double heterozygous mice. Diagram of allele specific CRISPR–Cas9 targeting of *Bcl2l11*. *Bcl2l11* was targeted using indicated gRNA sequences in one-cell embryos from a wild-type by *Morrbid*-deficient breeding. F1 mice with allele-specific *Bcl2l11* deletions in *cis* or in *trans* of the *Morrbid*-deficient allele were bred to a wild-type background to demonstrate linkage or segregation of *Bcl2l11* and *Morrbid* knockout alleles. Second-rightmost lanes of both gels contain *Morrbid*$^{-/-}$ *Bcl2l11*$^{+/+}$ DNA, and rightmost lanes contain water, as internal controls.

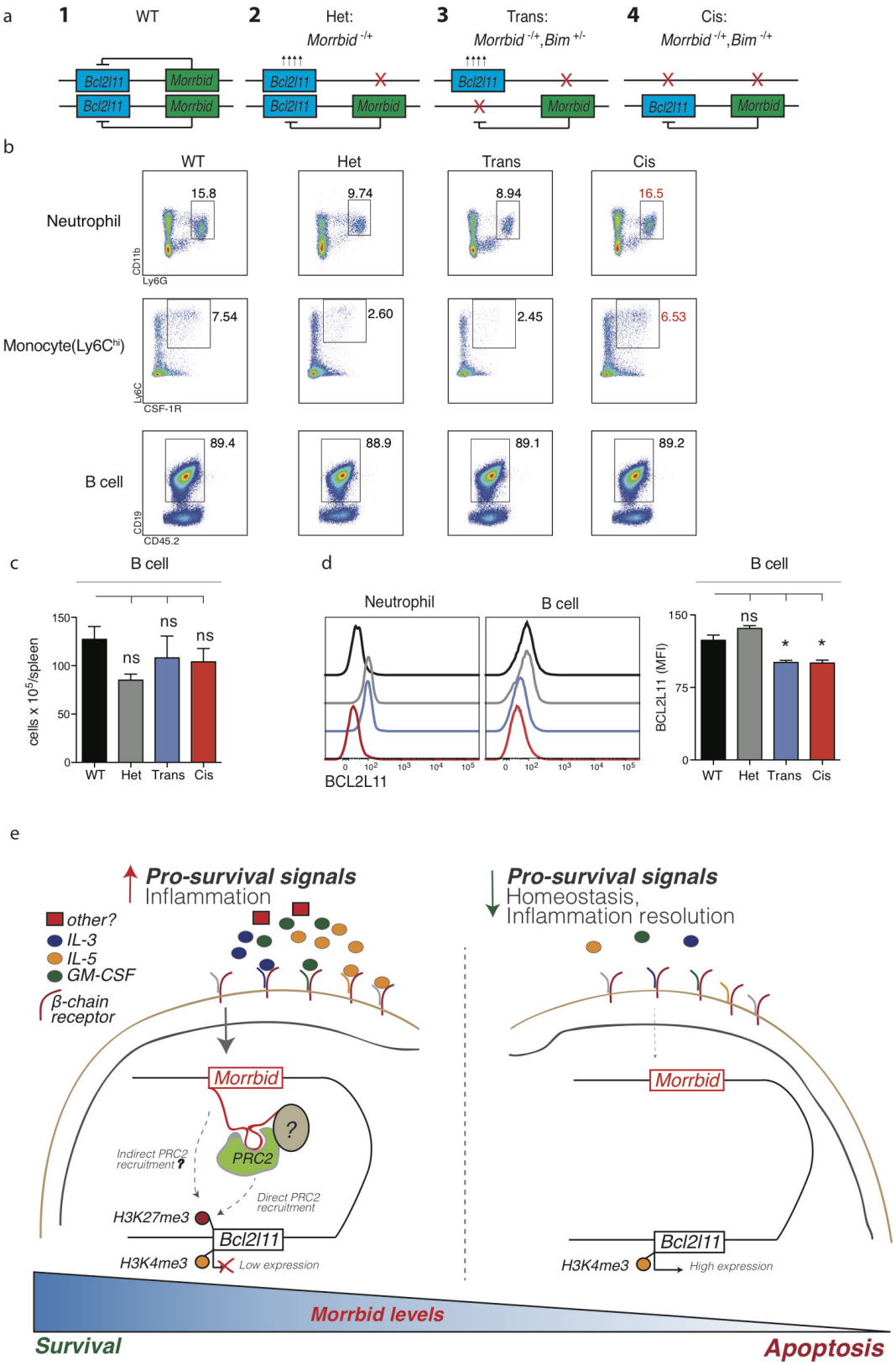

Extended Data Figure 10 | See next page for caption.

Extended Data Figure 10 | *Morrbid* regulates *Bcl2l11* in an allele-specific manner and working model of the role of *Morrbid*. **a**, Diagram of the allele-specific combinations of *Morrbid*- and *Bcl2l11*-deficient heterozygous mice studied. **b**, Representative flow cytometry plots of indicated splenic cell populations in the specified allele-specific deletion genetic backgrounds. Neutrophils ($CD45^+CD11b^+LY6G^+$), monoctyes ($CD45^+CD3^-CD19^-Ly6G^-SSC^{lo}SiglecF^-Ly6C^{hi}CSF\text{-}1R^+$) and B cells ($CD45^+Ly6G^-CD3^-CD19^+$). Wild-type (WT), *Morrbid* heterozygote (Het), *Bcl2l11* heterozygote and *Morrbid* heterozygote with deletions in *trans* (Trans), *Bcl2l11* heterozygote and *Morrbid* heterozygote with deletions in *cis* (Cis). **c**, **d**, Absolute counts (**c**) and BCL2L11 protein expression (**d**) of indicated splenic cell populations in the specified genetic backgrounds ($n = 3$–9 mice per genetic background). **e**, *Morrbid* integrates extracellular signals to control the lifespan of eosinophils, neutrophils and classical monocytes through the allele-specific regulation of *Bcl2l11*. Pro-survival cytokines induce *Morrbid*, which promotes enrichment of the PRC2 complex within the bivalent *Bcl2l11* promoter through direct and potentially indirect mechanisms to maintain this gene in a poised state. Tight control of the turnover of these short-lived myeloid cells by *Morrbid* promotes a balance of host anti-pathogen immunity with host damage from excess inflammation. Error bars show s.e.m. $^*P < 0.05$, $^{**}P < 0.01$, and $^{***}P < 0.001$ (one-way ANOVA with Tukey post-hoc analysis).